# RoboBoat 2026: Technical Design Report BlueHomeland Team

T. Yarkın USTA, Berkant GÜNİNDİ, M. Barış Hacim, Hasan H. ÇAM, Enes D. YALÇINKAYA, Özgür ÇOBAN, M. Cenk ÖZEKİNCİ, Doğuş ÖZKAN

*National Defence University, Turkish Naval Academy, Türkiye, İstanbul*

***Abstract*—Team BlueHomeland targets the RoboBoat 2026 title using a rigorous Evolutionary Prototyping workflow. Central to this strategy is a unique "Test Mule" methodology, utilizing a proxy platform to validate algorithms through high-frequency in-situ testing in the Naval Academy's inner harbor, eliminating the "Sim-to-Real" gap. The mechanical design features an optimized trimaran hull validated through Ansys Fluent computational fluid dynamics (CFD) analysis, ensuring hydrodynamic stability and minimized roll motion for superior sensor fidelity. Computationally, the system leverages an NVIDIA Jetson AGX Orin orchestrating a custom, lightweight Python architecture that bypasses ROS middleware to ensure a deterministic, low-latency control loop. Perception is maintained via a robust sensor fusion layer combining ZED 2i stereo depth, RPLIDAR scanning, and GPS, while the object detection achieved by a TensorRT-optimized YOLOv11 model that delivers a 5x inference speedup. Precise course-keeping is further guaranteed by a custom P-Control algorithm stabilized by Kalman filtering. Ultimately, this report demonstrates a system where every design decision is grounded in empirical data from real-world conditions.**

***Index Terms*—Autonomous Surface Vehicle, Computer Vision, Edge Computing, Evolutionary Prototyping, Sensor Fusion.**

ACRONYMS AND ABBREVIATIONS

| | |
|---|---|
| **ASV** | Autonomous Surface Vehicle |
| **CoG** | Center of Gravity |
| **EMI** | Electromagnetic Interference |
| **GCS** | Ground Control Station |
| **IMU** | Inertial Measurement Unit |
| **IVC** | Inter-Vehicle Communication |
| **MAVLink** | Micro Air Vehicle Link |
| **PWM** | Pulse Width Modulation |
| **RF** | Radio Frequency |
| **ROS** | Robot Operating System |

## I. COMPETITION STRATEGY

### A. Development Strategy

Due to the system's complexity and the dynamic structure of the marine environment, the Evolutionary Prototyping Model [1] was selected for the development of the Autonomous Surface Vehicle (ASV). This approach is particularly well-suited for embedded systems where defining full requirements upfront is difficult and where field testing is essential. The methodology begins with the rapid creation of a baseline prototype featuring core autonomous navigation and sensor capabilities. This prototype was tested not only in simulation environment but also sea and pool trials.

The implemented iterative process**,** as illustrated in Appendix A, Figure A.1, consists of the following stages:

**Quick Design and Coding:** Implementation of basic maneuvering capabilities and failsafe protocols.

**Prototype Integration:** Embedding the software onto the hardware platform.

**Field Testing (Sea Trials):** Observation of the vehicle's behavior under real-world marine conditions.

**Defect Analysis & Algorithm Refinement:** Analysis of log data acquired during testing (IMU, GPS, LiDAR), detection of software bugs, and optimization of algorithms.

This cycle was reiterated until the vehicle achieves the desired level of autonomy (Appendix A, Figure A.1, Optimum System). Consequently, hardware-software discrepancies that may not be apparent theoretically are identified at an early stage, thereby enhancing the reliability of the final version.

### B. Course Approach

Our strategy for the RoboBoat 2026 course was built upon the principle of "Reliable Autonomy," prioritizing tasks where our existing perception stack offers the highest probability of success while minimizing computational overhead.

We have carried forward our proven navigation architecture from the previous year, which utilizes a ZED

stereo camera for depth perception fused with a P-Control algorithm. Recent setup has demonstrated high stability in obstacle avoidance, requiring only minor adaptations to the computer vision pipeline to classify the new indicator buoys effectively.

The primary technical challenge we have identified is the "situational awareness" required during inter-task transitions. To address this, our main development focus is establishing a robust state-machine that utilizes GPS localization and local perception to distinguish between task zones. This ensures the ASV correctly identifies which specific mission protocol to execute.

In terms of task prioritization, the Speed Challenge is our primary objective. Given our system's rapid detection and reaction capabilities, we identified this as a high-reward, low-risk task to be completed firstly. Following this, our second priority is the Communications and Reports task. Since our vision system is already optimized for target acquisition and distance measurement, this task is reduced to a data transmission problem, which we will solve by integrating a dedicated sub-process to send data over Wi-Fi.

Conversely, resource-intensive tasks such as object delivery and water sampling will be approached opportunistically. Executing a dedicated search algorithm across the entire course area was deemed too costly in terms of time and battery life. Therefore, the ASV will only attempt these tasks if targets are detected within its immediate path or line of sight.

Finally, the Signal Blast and Docking tasks have been assigned the lowest priority. The complexity of mapping the harbor, identifying open bays, and the fusion required for sequence detection presents a high risk of mission failure; thus, these will only be attempted if the primary objectives are completed ahead of schedule.

### *C. Entry/Exit Gate & Navigation Channel*

The ASV initiates a sensor fusion algorithm combining ZED Stereo Camera, GPS, and LIDAR data for precise positioning. True heading is derived by stabilizing magnetic heading data with a Kalman Filter and correcting for local magnetic declination (-6.5° for Sarasota) [2].

The navigation strategy involves generating a linear path through the gates, followed by assigning GPS waypoints at 5 m intervals for the obstacle course. A real-time safety mechanism continuously scans obstacles using Lidar-Vision fusion. If an obstacle is detected within the safety radius, the ASV calculates a collision-free alternative route.

The mission concludes when the ASV identifies the green indicator buoy, executes a circumnavigation maneuver, and updates the system flags to transition seamlessly to Task 3.

### *D. Speed Challenge*

The system initiates a localization verification protocol to confirm the task starting position. This position is validated only when a gate buoy pair is detected, and no other red or green buoys are found within an approximate 5 m threshold of the pair.

Upon verification, a state-based control mechanism is implemented using the color class on the indicator buoy as a reference. The algorithm assigns a specific state based on the detected color, prompting the path planning module to dynamically generate a trajectory that passes on the side indicated by the indicator buoy (see Appendix B, Figure B.1).

### *E. Object Delivery*

The autonomous mission planner is designed to execute tasks sequentially; however, it incorporates a dynamic priority interruption mechanism for this task. If the perception system identifies the specific targets for this task within a proximity threshold of approximately 10 m —either during active navigation on the current route or during inter-task transitions— the current mission state and coordinates are temporarily cached. The vehicle then deviates to execute and complete object delivery.

Upon successful completion, the system retrieves the saved coordinates, returns to the point of interruption, and resumes the original task sequence (see Appendix B, Figure B.2).

### *F. Docking*

The ASV executes a two-phase strategy comprising identification and maneuvering. Initially, the system performs an iterative inspection of each potential docking bay. During this scan, the perception module extracts and records both the indicator color and the numerical value displayed at each station. Once the data acquisition is complete, the decision algorithm processes the recorded entries to identify the target bay characterized by a green indicator associated with the lowest numerical value.

Upon target confirmation, the path planner generates a precision approach trajectory to dock into the selected bay, followed immediately by a reverse maneuver to safely exit the structure.

### *G. Sound Signal*

A frequency discrimination algorithm is implemented to analyze the spectral properties of incoming audio data. The algorithm filters ambient noise to detect predominant frequencies within 500-1200hz. Upon detection, the system maps the signal to a corresponding operational state: one signal triggers 'State 1', while two signals

trigger 'State 2'. Each state is associated with a distinct set of global coordinates. Once the state is set, the ASV navigates to the assigned location.

Upon arrival, the perception system identifies the yellow buoy closest to the target coordinates, approaches it, and executes the specific sub-algorithm dedicated to that acoustic task (see Appendix B, Figure B.3).

### *H. Communications & Reporting*

The ASV is equipped with a comprehensive data logging and reporting architecture designed to meet the automated reporting requirements of the autonomy challenge. The system processes sensor data in real-time to extract task-specific metrics, which are then queued for transmission to the GCS (Ground Control Station).

#### *1) Data Collection & Processing*

**Task 1 (Navigation Channel):** The system validates gate traversal by monitoring the vehicle's proximity to the gate markers. When the distance to the gate pair falls below 2 m, a "traversal event" is triggered, logging the current timestamp and GPS coordinates to confirm the passage.

**Task 2 (Object Avoidance)**: To report obstacle locations, the system employs a sensor fusion approach. Object detection model(YOLO) identifies the buoy, while the ZED stereo camera provides depth data. This local relative position is transformed using the vehicle's instantaneous global position and heading to calculate and record the absolute coordinates of each buoy.

**Task 3 (Speed Challenge):** The specific buoy color is identified via YOLO. Simultaneously, a software-based chronograph measures the elapsed time for the circuit. The timer starts when the vehicle exits the starting GPS geofence and halts upon its second arrival at the same coordinate set.

**Task 4 & 5 (Object Delivery & Docking):** Similar to Task 2, the system utilizes YOLO and ZED depth sensing to identify and log the target's color alongside its georeferenced location.

**Task 6 (Sound Signal):** Upon activation (when the audio threshold is breached), the signal processing module logs the detected signal pattern (1 or 2 blasts), the specific frequency value, the assigned target task, and the timestamp of the detection event.

#### *2) RF Transmission Architecture*

A dedicated transmission algorithm runs in parallel with the primary autonomy stack to ensure that reporting does not introduce latency to the control loop. All logged data is serialized and sent in real-time via an integrated RF telemetry hardware module to the GCS in a range of 40 km [3].

## II. Design Strategy

### *A. Mechanical Structure*

In the hull concept selection phase, which forms the foundation of the mechanical design process, SWATH, catamaran, and trimaran forms were evaluated through a comprehensive literature review and preliminary analyses [4]. The final decision was driven by the pursuit of an optimal design, prioritizing criteria such as stability, equilibrium, speed, maneuverability, and the minimization of hydrodynamic forces and pressures acting on the hull structure, as validated by the CFD simulations detailed in Appendix C.

Crucially, for autonomous systems, minimizing vertical and rotational accelerations is a prerequisite to ensure the reliable operation of the sensor fusion suite. Considering the wave impacts the vessel will encounter, minimizing pitch motion was identified as a critical requirement to maximize sensor data fidelity. Consequently, the trimaran hull concept was selected due to its slender side hulls (outriggers), which reduce hydrodynamic drag, and its inherent high stability derived from the triple-hull configuration. This configuration significantly dampens roll motion while assisting in course-keeping stability during rough sea conditions.

Following the definition of the hull geometry, engineering efforts focused on the Center of Gravity(KG), the most critical factor determining hydrostatic equilibrium. To increase the Metacentric Height(GM) — the primary indicator of resistance to capsizing— the center of gravity was positioned at the lowest possible point along the vertical Z-axis [5]. This strategy maximizes the vessel's positive stability, ensuring a strong righting moment to return to an upright position when subjected to external heeling forces such as wind or waves.

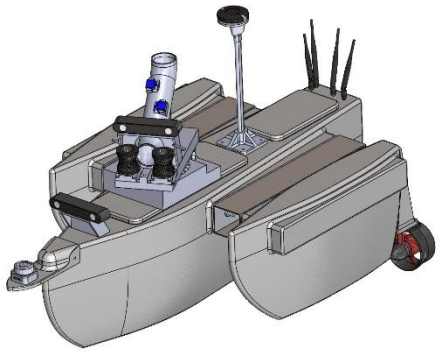

**Fig. 1:** Integrated CAD model of the trimaran hull.

### *B. Propulsion*

Two Degz Ultras thrusters were selected due to their high thrust-to-weight ratio [6]. The configuration of these thrusters was treated not merely as a means of propulsion,

but as a critical design parameter directly influencing the vehicle's dynamic behavior. The thrusters are positioned equidistantly on the starboard and port sides relative to the CoG. This symmetrical layout eliminates involuntary yaw moments during straight-line navigation. Simultaneously, it enables high maneuverability without the need for a mechanical rudder system, achieved through differential thrust applied to the motors [7].

### *C. Water Delivery Module*

The water delivery module is driven by a Bosch TMS 41210030081 (0986337402) wiper motor, selected for its high torque capacity and industrial-grade durability. Power is supplied via the 12V rail of the Matek PDB (Power Distribution Board). The actuation trigger is managed by a Solid-State Relay (SSR), controlled directly by the NVIDIA Orin Nano. To ensure stable relay operation, the Orin Nano's 3.3V GPIO signal is amplified through a custom 2N2222 NPN transistor circuit, guaranteeing reliable switching underload.

### *D. Racquetball Delivery Module*

The integrated firing system operates using real-time target data acquired from the ZED 2i camera. Precision control of the turret's lateral axis (yaw) is achieved via a NEMA 17 stepper motor, driven by a TMC2208 silent stepper driver to ensure smooth and accurate positioning.

The ammunition feeding mechanism utilizes three servo motors managed by a PCA9685 PWM driver, while the propulsion (launch) phase is executed by high-RPM brushless motors coupled to conical cylinders. To prevent electromagnetic interference (EMI) from disrupting the sensitive avionics, this entire subsystem is powered by an isolated, dedicated 7S LiPo battery.

### *E. Electrical System*

The electrical system is architected upon a "Split Power Topology," ensuring galvanic isolation between the high-current propulsion circuit and the sensitive avionics bus [8]. This segregation is critically protected by Solid State Relays (SSR) and fast-acting glass fuses to prevent current surges from damaging logic components; the comprehensive electronic schematic illustrating this architecture is provided in Appendix D.

Computational duties are divided hierarchically: the NVIDIA Jetson AGX Orin serves as the central mission computer, handling high-level tasks such as multi-sensor fusion (ZED 2i Depth/IMU/Magnetometer + LiDAR + HerePro GPS + Deity V-Mic D3 Pro Microphone) and autonomous decision-making algorithms. In contrast, the Pixhawk Orange Cube operates solely as a low-level actuator interface, isolating the motor control loop from high-level processing.

To guarantee uninterrupted data integrity, the communication infrastructure employs RFD telemetry modules, selected for their resilience against electromagnetic interference (EMI) and higher ranges. Simultaneously, high-bandwidth video streaming and mission data transfer are established using an Ubiquiti (Rocket M5 & LiteBeam) configuration, ensuring a robust link even in signal-saturated environments.

### *F. Perception*

The perception layer is the cornerstone of the ASV's autonomy, responsible for gathering, processing, and interpreting environmental data to ensure situational awareness and precise localization. Our team has designed a hybrid perception architecture that integrates computer vision, LiDAR scanning, and GPS positioning to successfully identify this year's task elements such as navigation and indicating buoys, docking bays, and object delivery targets.

The software stack is built upon NVIDIA JetPack 6.1, which provides a comprehensive development environment optimized for the Jetson AGX Orin. JetPack 6.1 integrates the Ubuntu 22.04 LTS operating system with the latest CUDA 12.6 drivers and the TensorRT library, ensuring maximum hardware efficiency for object detection [9].

To achieve real-time performance on the embedded platform, the custom trained YOLOv11 [10] object detection model is converted into a TensorRT engine ( .engine). This process optimizes the model for FP16 (half-precision) inference, significantly reducing latency and memory usage while maintaining high detection accuracy. According to benchmarks on Jetson AGX Orin, this optimization delivers an inference speedup of up to 5x compared to standard PyTorch execution [11].

The perception pipeline executes a synchronized workflow to translate raw sensor data into actionable navigation commands:

**Visual Object Detection:** Images captured are processed by the YOLOv11 algorithm to detect task objects.

**Spatial Analysis & Depth Extraction:** The center point of each detected object's bounding box is mapped to the ZED camera's depth map. Using the ZED SDK's depth.get_value() [12] API call, the system extracts the precise distance and 3D coordinates (x, y, z) of the object relative to the boat. This also allows the ASV to calculate the exact heading required to approach a target or navigate through the obstacles.

**Lidar Data Integration:** Raw scan data from the RPLIDAR S3 is processed using the rplidar [13] library. This data is converted into a local point cloud to identify immediate obstacles that may not be within the camera's

field of view or to confirm the distance of visually detected objects.

*G. Navigation*

The Navigation module orchestrates autonomy by synthesizing localization, mapping, and path planning. Localization is performed by fusing HerePro GPS data with ZED 2i magnetometer readings, refined by a 1D Kalman Filter [14] to eliminate magnetic noise. For mapping, a "Lidar-First" priority logic utilizes the RPLIDAR S3's stability, while the ZED camera covers blind spots; Lidar data serves as the authoritative ground truth during sensor discrepancies. The path planner establishes a virtual vector toward the waypoint, utilizing a lightweight A* algorithm [15] for obstacle avoidance within a set safety radius. To ensure smooth trajectory tracking and prevent sharp oscillations, the system follows a look-ahead point, effectively a virtual target positioned 1 meter ahead on the path, which guides the ASV's steering and maintains fluid course corrections.

*H. Control*

The control layer, hosted on an NVIDIA Jetson AGX Orin, translates high-level path commands into thruster signals. Communication with the OrangeCube flight controller is established via a USB interface using the MAVLink protocol [16] and the pymavlink API [17] for robust, low-latency data exchange. This setup enables a custom Proportional (P) Gain Controller to manage the ASV's heading and speed. By leveraging the hull's hydrodynamic damping, the controller minimizes computational load while calculating differential thrust based on the error between the desired bearing and the filtered ZED magnetometer heading. Finally, the OrangeCube converts these MAVLink commands into PWM signals for the ESCs to execute course corrections.

*I. Software Architecture*

The software architecture of the ASV is structured around a linear Input-Process-Output model, adopting the classical Sense-Plan-Act (SPA) paradigm [18]. This framework is designed to transform raw environmental data into precise physical actuation. As illustrated in the system flow diagram (see Appendix E), the architecture is divided into three distinct layers: Perception (Input/Sense), Navigation & Control/Decision-Making (Process/Plan), and Action (Output/Act). This entire pipeline is executed on the NVIDIA Jetson AGX Orin.

Upon power-up, the input layer asynchronously fuses sensor data using the Multiprocessing library. These estimates are fed into the process layer's Mission Planner state machine, which generates the navigation commands executed by the output layer.

While the Robot Operating System (ROS) is a prevalent standard in the domain, a custom modular Python architecture is strategically adopted. By bypassing the heavy middleware overhead and serialization complexities inherent to ROS, we aimed to achieve a more lightweight and deterministic system. Comparative studies on inter-process communication have shown that standard ROS implementations can introduce higher latency compared to lightweight or native data exchange mechanisms, especially under high-frequency control loops [19].

To manage concurrent operations, parallelism is handled explicitly via the Python Multiprocessing library [20]. This approach enables sensor drivers and sub-algorithms to execute asynchronously on isolated cores. By leveraging the NVIDIA Jetson AGX Orin's multi-core architecture directly, this method eliminates middleware-induced latency and serialization bottlenecks. The result is a streamlined, target-oriented development workflow that significantly reduces debugging time while ensuring real-time responsiveness.

*J. Inter-Vehicle Communication*

To maintain a rigorous development schedule for this year's competition, a dual-platform strategy is employed. The primary Vehicle 1 is currently under construction as the main competition craft, while the previous year's hull serves as a "test mule" (Vehicle 2) to facilitate ongoing field trials and software validation. Both platforms utilize a standardized electronic architecture to ensure code portability, with two key hardware exceptions: Vehicle 2 is equipped with an NVIDIA Jetson Orin Nano (replacing the AGX Orin) and lacks the mission-specific shooter mechanisms.

Furthermore, Ubiquiti networking hardware is exclusive to Vehicle 1 to manage high-bandwidth camera streams and redundant GCS communication. This infrastructure is omitted on Vehicle 2, which instead focuses on GPS-based formation tracking by following reference coordinates provided by the primary vehicle. This multi-vehicle deployment is designed to secure additional Inter-Vehicle Communication (IVC) points while enabling Vehicle 2 to assist in mission tasks. Specifically, Vehicle 2 performs local mapping and object detection, transmitting the fused results to Vehicle 1 to enhance overall situational awareness.

Communication is facilitated by RFD900x telemetry through a transparent serial UART interface. The system utilizes a three-node broadcast topology governed by a custom protocol to prevent data collisions. By prepending a unique identification header to each packet, the receiving unit can authenticate the data source in real-time. This mechanism ensures packet integrity and

enables synchronized, conflict-free coordination between the autonomous platforms during complex maneuvers.

### *K. Ground Control Station*

The Ground Control Station (GCS) is a custom application developed in Python, utilizing the PySide6 framework [21] for real-time monitoring and mission management. The system is built on a robust, standalone architecture designed to operate independently of external internet connections, ensuring mission continuity in isolated environments. For the long-range communication infrastructure via RFD900x telemetry modules, a raw serial communication scheme was prioritized over complex standard protocols. Instead of adopting the heavy header structures of TCP/IP or the strict definitions of MAVLink for this specific link, data packets are structured in JSON format. This provides high flexibility for rapid protocol iteration. To ensure the graphical user interface (GUI) remains responsive and freeze-free, all blocking I/O operations are executed on asynchronous worker threads managed by the QThread class [22].

A key feature of the system is its offline mapping engine, developed to mitigate potential connectivity issues at the competition venue. Without relying on external libraries, the software utilizes embedded WebMercator projection formulas to convert GPS coordinates into pixel coordinates on local map images [23]. Furthermore, high-resolution field maps are processed using a custom tiled rendering algorithm. This technique optimizes memory management by loading map segments dynamically, ensuring fluid visualization even at high zoom levels. The complete source code for this rendering engine and projection implementation is available in our repository [24].

To enhance operational safety, the interface is divided into two main panels: numerical telemetry data and visual map tracking. The vehicle's track, true heading, and target heading are rendered in real-time as vector graphics on the map, while keyboard integration allows the operator to switch to manual control within milliseconds if necessary. Furthermore, the system includes a dedicated "Emergency Stop" mechanism designed to transmit a high-priority signal that immediately disables the vehicle's propulsion system, while all mission data is logged in CSV format for post-operation analysis.

## III. TESTING STRATEGY

Our team adopts an agile, "Test-Fix-Deploy" methodology that prioritizes high-fidelity, real-world data collection over synthetic simulation. While simulation is common in the industry, our team utilizes a unique logistical advantage: direct daily access to the Naval Academy's private boathouse and a calm inner harbor. This accessibility allows us to eliminate the "Sim-to-Real gap" entirely, ensuring that our algorithms are validated against actual maritime dynamics, lighting conditions, and physical disturbances from day one.

To optimize development time and decouple software readiness from mechanical manufacturing, we employ a "Test Mule" strategy [25]. We utilize our previous generation hull (Teknofest 2025 ASV) as a robust testing platform. While the new RoboBoat 2026 hull is undergoing design analysis and manufacturing, the complete 2026 electronics suite has been retrofitted onto the Mule. This allows the software team to validate the Perception, Decision, and Control layers in the water months before the final hull is launched. Once the 2026 hull is ready, the fully matured software stack will be transferred with minimal integration friction.

To ensure system reliability and mitigate the risks associated with rapid prototyping, a structured, multi-phase testing framework has adopted. This incremental approach allows us to validate individual subsystems in isolation before integrating them into the complex autonomous architecture. The process begins with **"**Dry Bench**"** component testing to verify hardware logic, progresses to "Dockside Integration" checks for waterproofing and connectivity, and culminates in "Mission Simulation" where full autonomous behaviors are rigorously evaluated in the inner harbor. This hierarchical structure ensures that critical failures are identified and resolved at the lowest possible level, preventing costly setbacks during full-mission simulations. Table 1 provides a summary of these development phases and their current status. For a comprehensive breakdown of the timeline, quantitative results, and the risk assessment framework governing these operations, please refer to Appendix F (Team Gantt Chart), Appendix G (Task Plan and Results), and Appendix H (Risk Management), respectively.

**Table 1:** Summary of Development Phases and Testing Status

| Phase | Period | Activity | Status |
|---|---|---|---|
| **Phase I** | Oct 1 – Oct 20 | **Dry Bench Testing**: Sensor Configuration, dependencies setup | Completed |
| **Phase II** | Oct 20 – Nov 15 | **Dockside Integration:** GCS communication tests, fail-safe verification | Completed |
| **Phase III** | Nov 15 – Dec 1 | **Inner Harbor Tests & Tunings:** P-Controller tuning, Perception & Navigation algorithm setups | Completed |
| **Phase IV** | Dec 1 – Feb 1 | **Mission Simulation:** Full autonomy runs and refinements on mock courses using the "Mule" | In Progress |
| **Phase V** | Feb 1 – Feb 15 | **Final Migration:** Transferring validated electronics to the new hull | Planned |

## ACKNOWLEDGMENTS

We sincerely thank our faculty advisor, Assoc. Prof. Doğuş Özkan, for his critical guidance on project management and mechanical solutions. We specifically thank Rear Admiral Ramazan Özoğul (Commander of the Turkish Naval Academy) for authorizing 24/7 access to the inner harbor and ship model testing pool for trials, as well as providing full use of the R&D (Research and Development) and Mechatronics laboratories for 3D printing and vehicle assembly.

Our project was further strengthened by industry and financial support. We thank Yonca Shipyard (Yontech) for manufacturing and coating the outer hull. Finally, we acknowledge the generous financial funding from ASFAT, SUPRA DEFENCE, Tübitak, Turkish Airlines and our Dean, Prof. Dr. Cemalettin Şahin, which enabled the procurement of essential electronic components and resources.

## REFERENCES

[1] I. Sommerville, *Software Engineering*, 10th ed. Pearson, 2015, pp. 28–30.

[2] National Oceanic and Atmospheric Administration (NOAA), "Magnetic Field Calculators," 2025. [Online]. Available: https://www.ngdc.noaa.gov/geomag/calculators/magcalc.shtml.

[3] RFDesign, "RFD900x Ultra Long Range Telemetry Modem Datasheet," 2023. [Online]. Available: http://files.rfdesign.com.au/Files/documents/RFD900x%20Data Sheet.pdf.

[4] R. Dubrovsky and A. Lyakhovitsky, *Multi-Hull Ships*. Backbone Publishing, 2001.

[5] E. V. Lewis, Ed., *Principles of Naval Architecture: Volume I - Stability and Strength*. Jersey City, NJ: Society of Naval Architects and Marine Engineers, 1988.

[6] Degz Robotics, "Utras Thruster Technical Details," 2024. [Online]. Available: https://degzrobotics.com/product/utras_rov_auv_vessel_underwater_thruster

[7] T. I. Fossen, *Handbook of Marine Craft Hydrodynamics and Motion Control.* Chichester, UK: John Wiley & Sons, 2011.

[8] P. Horowitz and W. Hill, *The Art of Electronics*, 3rd ed. Cambridge, UK: Cambridge University Press, 2015.

[9] NVIDIA Corporation, NVIDIA JetPack SDK 6.1 Release Notes and Documentation. Santa Clara, CA: NVIDIA Corp., 2024. [Online]. Available: https://developer.nvidia.com/embedded/jetpack

[10] G. Jocher et al., "Ultralytics YOLO," Ultralytics, 2025. [Online]. Available: https://github.com/ultralytics/ultralytics

[11] Ultralytics, "NVIDIA Jetson Guide: Jetson AGX Orin Developer Kit Benchmarks," Ultralytics Docs, 2024. [Online]. Available: https://docs.ultralytics.com/guides/nvidia-jetson/#nvidia-jetson-agx-orin-developer-kit-64gb

[12] Stereolabs, "Using the Depth Sensing API," Stereolabs Docs, 2025. [Online]. Available: https://www.stereolabs.com/docs/depth-sensing/using-depth

[13] Skoltech Robotics, "rplidar: Simple and lightweight module for RPLIDAR," GitHub Repository, 2024. [Online]. Available: https://github.com/SkoltechRobotics/rplidar

[14] G. Welch and G. Bishop, "An Introduction to the Kalman Filter," University of North Carolina at Chapel Hill, Chapel Hill, NC, USA, Tech. Rep. TR 95-041, 2006. [Online]. Available: https://www.cs.unc.edu/~welch/media/pdf/kalman_intro.pdf

[15] P. E. Hart, N. J. Nilsson, and B. Raphael, "A Formal Basis for the Heuristic Determination of Minimum Cost Paths," *IEEE Transactions on Systems Science and Cybernetics*, vol. 4, no. 2, pp. 100–107, 1968.

[16] MAVLink, "MAVLink Developer Guide," *MAVLink.io*, 2024. [Online]. Available: https://mavlink.io/en/

[17] ArduPilot, "Pymavlink: Python MAVLink implementation," *ArduPilot Developer Documentation*, 2024. [Online]. Available: https://ardupilot.org/dev/docs/pymavlink.html

[18] R. R. Murphy, "The Hierarchical Paradigm," in *Introduction to AI Robotics*, 2nd ed. Cambridge, MA, USA: MIT Press, 2019, pp. 27–30.

[19] P. B. Sousa, A. P. Moreira, and P. Costa, "Performance Analysis of Inter-Process Communication Mechanisms in Robotic Systems," in *Proceedings of the 2016 IEEE International Conference on Autonomous Robot Systems and Competitions (ICARSC)*, Braganca, Portugal, 2016, pp. 27–32.

[20] Python Software Foundation, "multiprocessing — Process-based parallelism," *Python 3.12 Documentation*, 2024. [Online]. Available: https://docs.python.org/3/library/multiprocessing.html

[21] The Qt Company, "Qt for Python (PySide6) Documentation," *Qt.io*, 2024. [Online]. Available: https://doc.qt.io/qtforpython-6/

[22] The Qt Company, "QThread Class Reference," *Qt.io*, 2024. [Online]. Available: https://doc.qt.io/qt-6/qthread.html

[23] National Geospatial-Intelligence Agency (NGA), "Implementation Practice Web Mercator Map Projection," NGA Standardization Document, Version 2.0, 2014. [Online]. Available: https://earth-info.nga.mil/

[24] T. Y. Usta, "GCS: Ground Control Station for ASV," *GitHub Repository*, 2025. [Online]. Available: https://github.com/tolgayarkinusta/GCS

[25] K. T. Ulrich and S. D. Eppinger, "Prototyping," in *Product Design and Development*, 6th ed. New York, NY, USA: McGraw-Hill Education, 2016, pp. 291–310.

APPENDIX A

**Evolutionary Prototyping Process Flow**

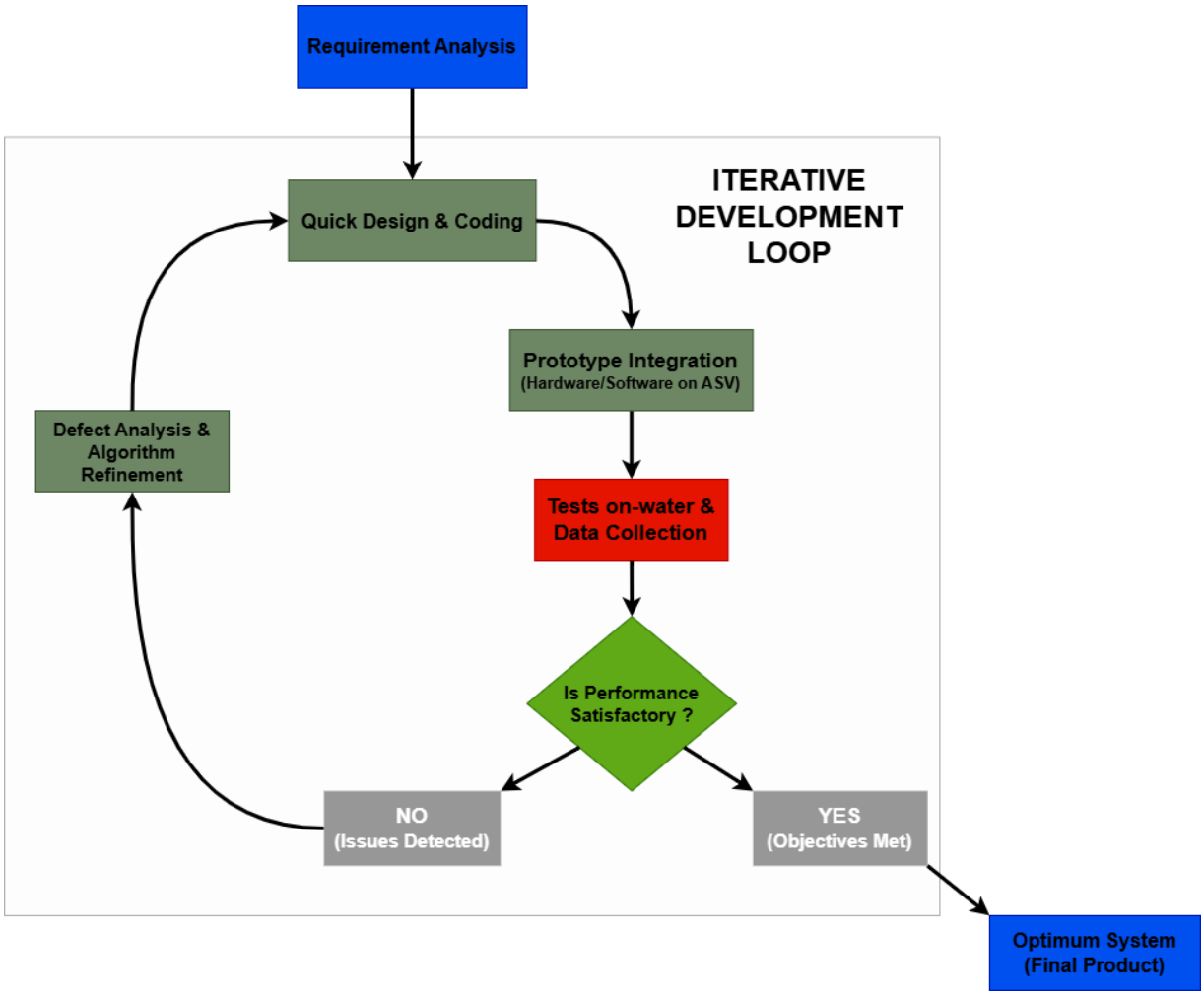


**Fig. A.1:** Flowchart of the Evolutionary Prototyping Model used for the ASV development.

## APPENDIX B

## Autonomy Algorithm Flowcharts

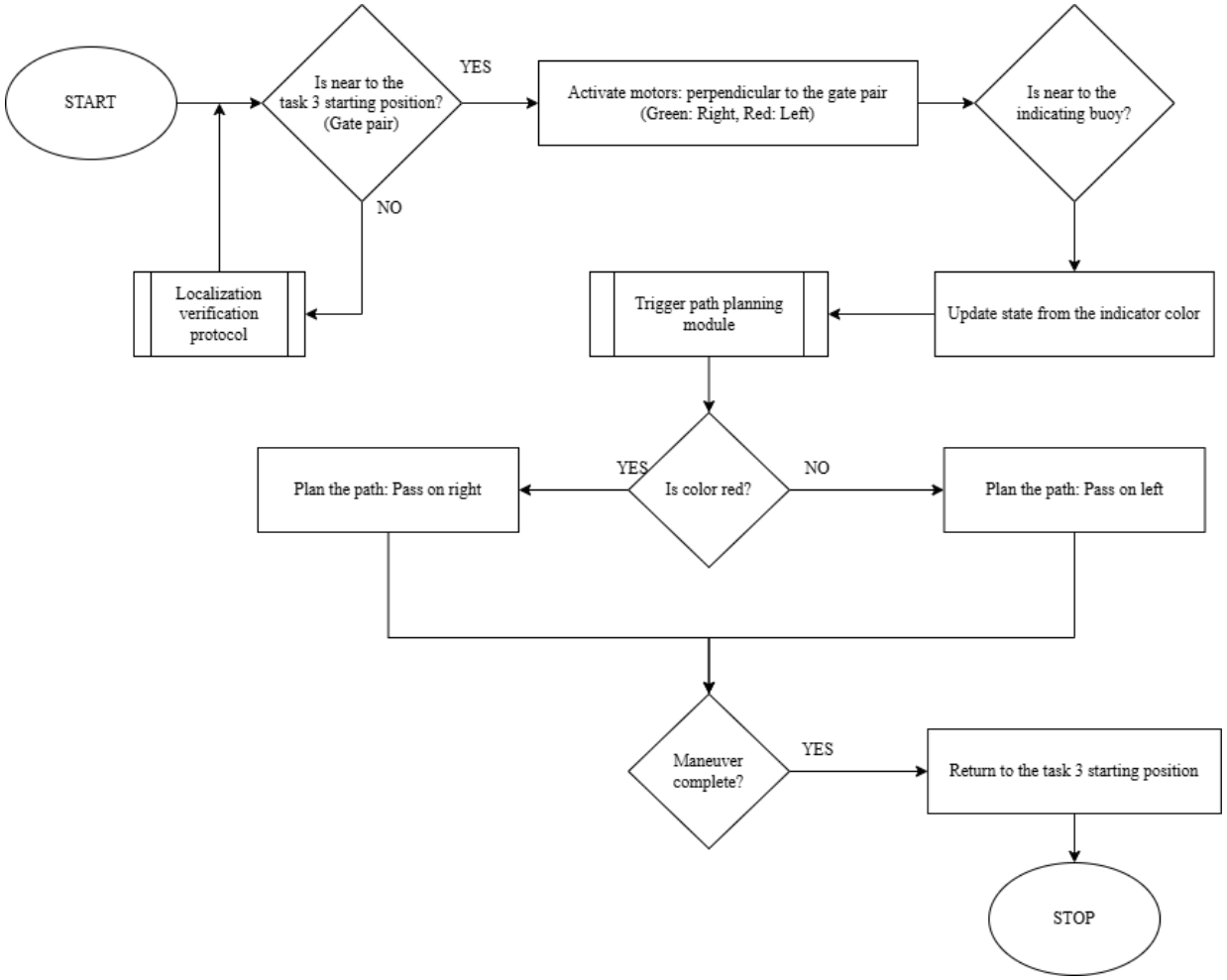


**Fig. B.1:** Speed Challenge Algorithm Flowchart

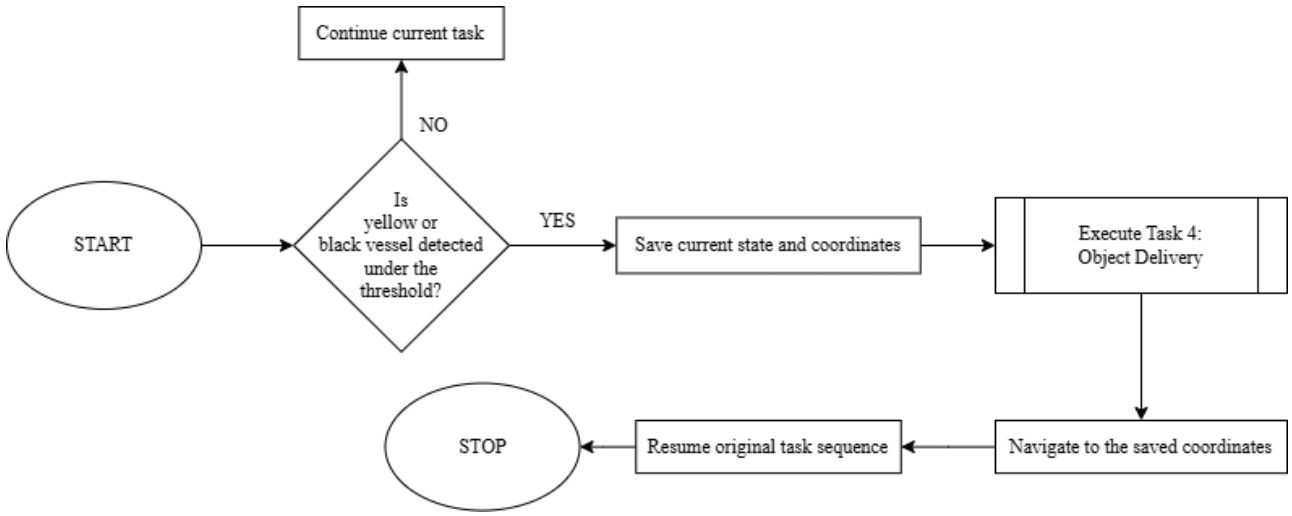


**Fig. B.2:** Object Delivery Algorithm Flowchart

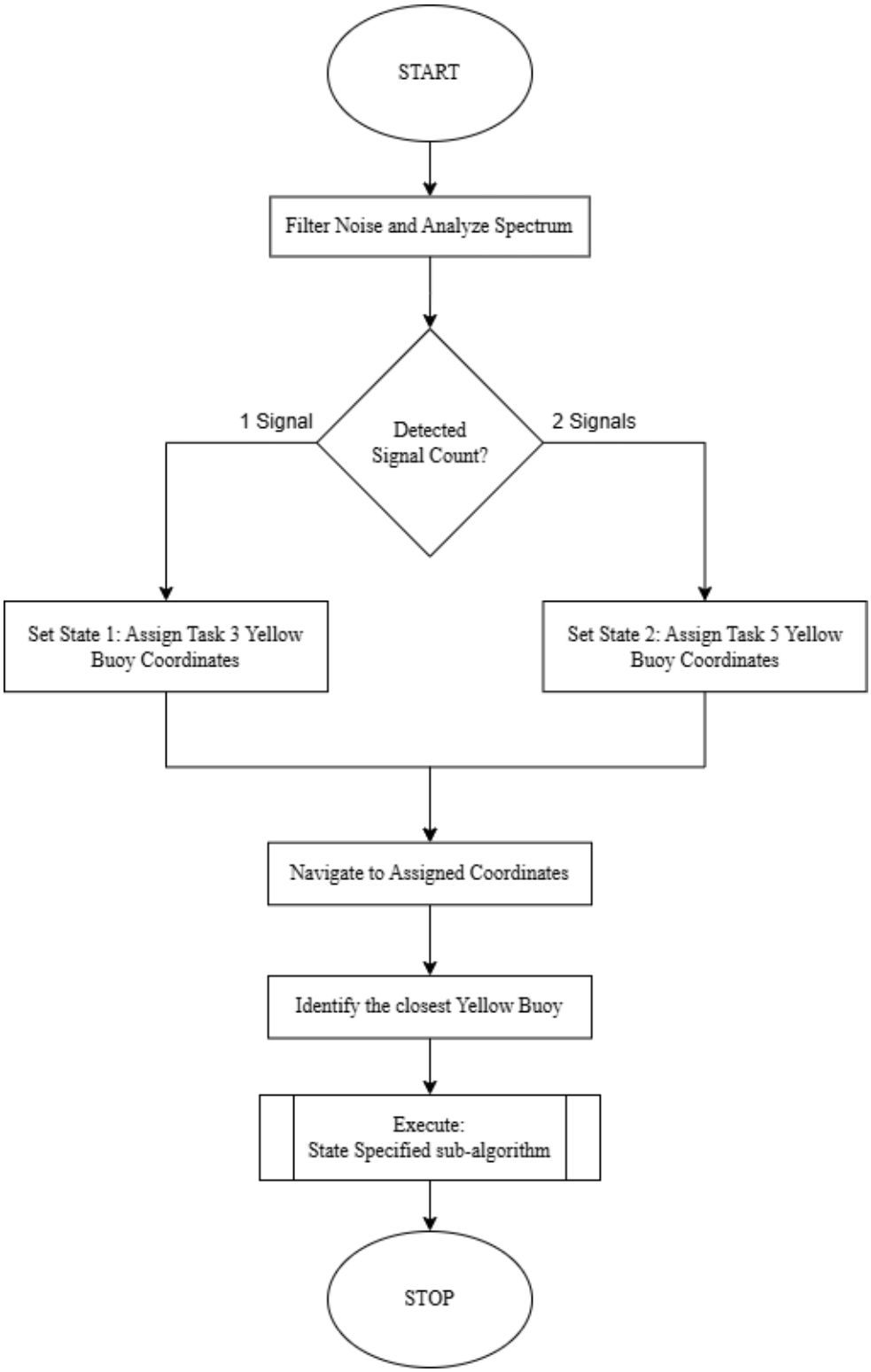


**Fig. B.3:** Sound Signal Algorithm Flowchart

APPENDIX C

## Computational Fluid Dynamics (CFD) Analysis & Hull Optimization

The complex requirements of the RoboBoat competition, specifically autonomous navigation stability, obstacle avoidance maneuvers, and the energy efficiency required for extended operations, necessitated an ASV design optimized specifically for the mission profile, rather than relying on a standard hull form. Consequently, before physical manufacturing commenced, an iterative and multi-stage Computational Fluid Dynamics (CFD) process was conducted to maximize hydrodynamic performance, minimize drag forces, and guarantee dynamic stability.

Instead of a linear progression, the design and analysis methodology was executed in three feedback-loop phases:

### Phase 1: Hull Topology and Form Optimization

The initial design phase focused on the "bare hull" geometry as illustrated in Figure C.1. Various hull forms (including catamaran, trimaran, and monohull variations) were evaluated based on their wet surface areas and form drag coefficients to identify the most hydrodynamically efficient geometry. At this stage, hardware weights were excluded to prioritize the prevention of flow separation and the maintenance of laminar flow (see Figure C.2).

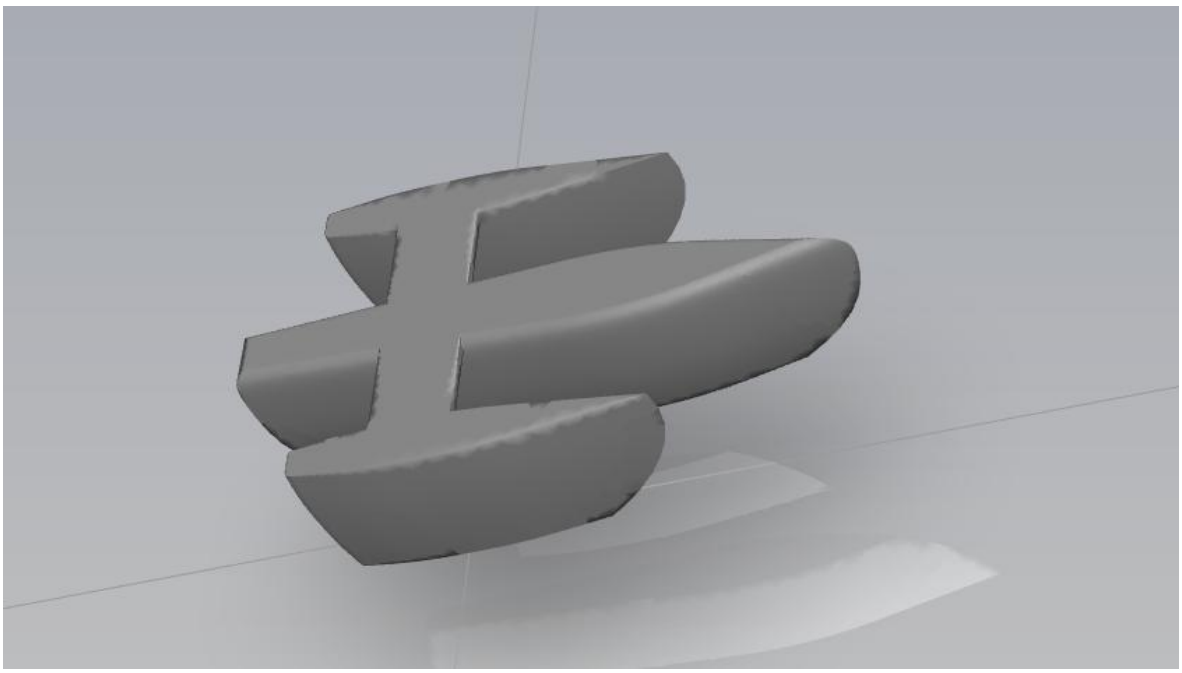

**Fig. C.1:** CAD of the “bare hull”

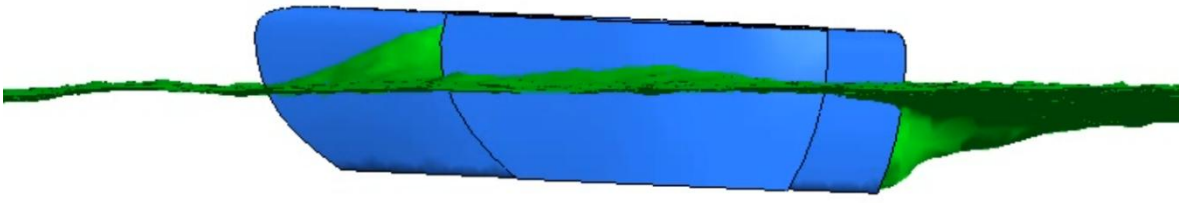

**Fig. C.2:** Stability and buoyancy Analysis of the “bare hull” via ANSYS Fluent

**Phase 2: Full Load Displacement and Center of Gravity (CoG) Analysis**

Following the definition of the hydrodynamic form, all mechanical and electronic systems (LiDAR, ZED stereo camera, battery blocks, main control boards) were integrated into the model as illustrated in Figure C.3. Total weight and moments of inertia, calculated within SolidWorks, were directly applied to the CFD boundary conditions. Analysis was repeated using the actual mass distribution rather than just geometry; by optimizing the vertical (KG) and longitudinal (LCG) positions of the center of gravity, the vessel's static equilibrium and draft were verified in the virtual environment.

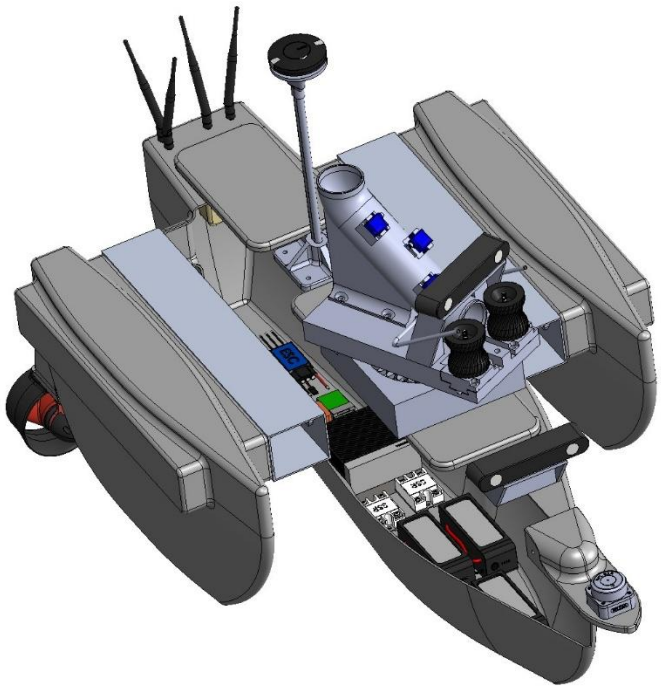

**Fig. C.3:** Integration of electronical and mechanical components for mass distribution and Center of Gravity (CoG) verification.

**Phase 3: Propulsion Integration and Stabilization Strategy**

Determining the position and angle of the motors relative to the hull was the most critical phase of the analysis. CFD results indicated a tendency for slight porpoising and trim-up behavior at cruising speeds. To dampen this hydrodynamic instability, a passive, permanent solution was developed rather than relying on active control surfaces:

- Thrusters were positioned to create an optimum moment arm relative to the hull centerline.
- A specific negative tilt (thrust vectoring) was applied to the motor mounting angle, opposing the hull axis. Through this strategic angulation, the vertical component of the thrust force generates a counter-moment that pushes the bow down, converging the trim angle to near zero during navigation. This maximizes the data collection stability of onboard sensors, particularly the LiDAR and cameras.

ANSYS Fluent was selected as the solver due to its proven capability to model these complex physical interactions, free surface deformations (VOF Method), and 6-DOF vessel motions with high accuracy using industrial-grade turbulence models (k-omega SST) and dynamic mesh infrastructure. The numerical data obtained confirms that the designed vehicle has reached the hydrodynamic maturity required for RoboBoat missions.

**Mesh Structure**

The general topology of the computational grid employed for the CFD simulations is presented in Figure C.4. To ensure that the flow physics surrounding the hull remains uncorrupted by boundary effects, the computational domain was established with sufficient far-field extent.

A critical feature illustrated in the mesh structure is the high-density refinement zone applied along the free surface line, where the water and air phases intersect. Element sizes within this specific band were strictly minimized to enable the Volume of Fluid (VOF) method to accurately resolve wave propagation and the phase interface. Comprising a total of 3.3 million elements, this hybrid mesh structure was engineered to strike an optimum balance between computational cost and solution fidelity. Accordingly, element sizes were gradually coarsened (inflation layers) in the far-field regions where flow gradients are negligible, focusing computational resources where they matter most.

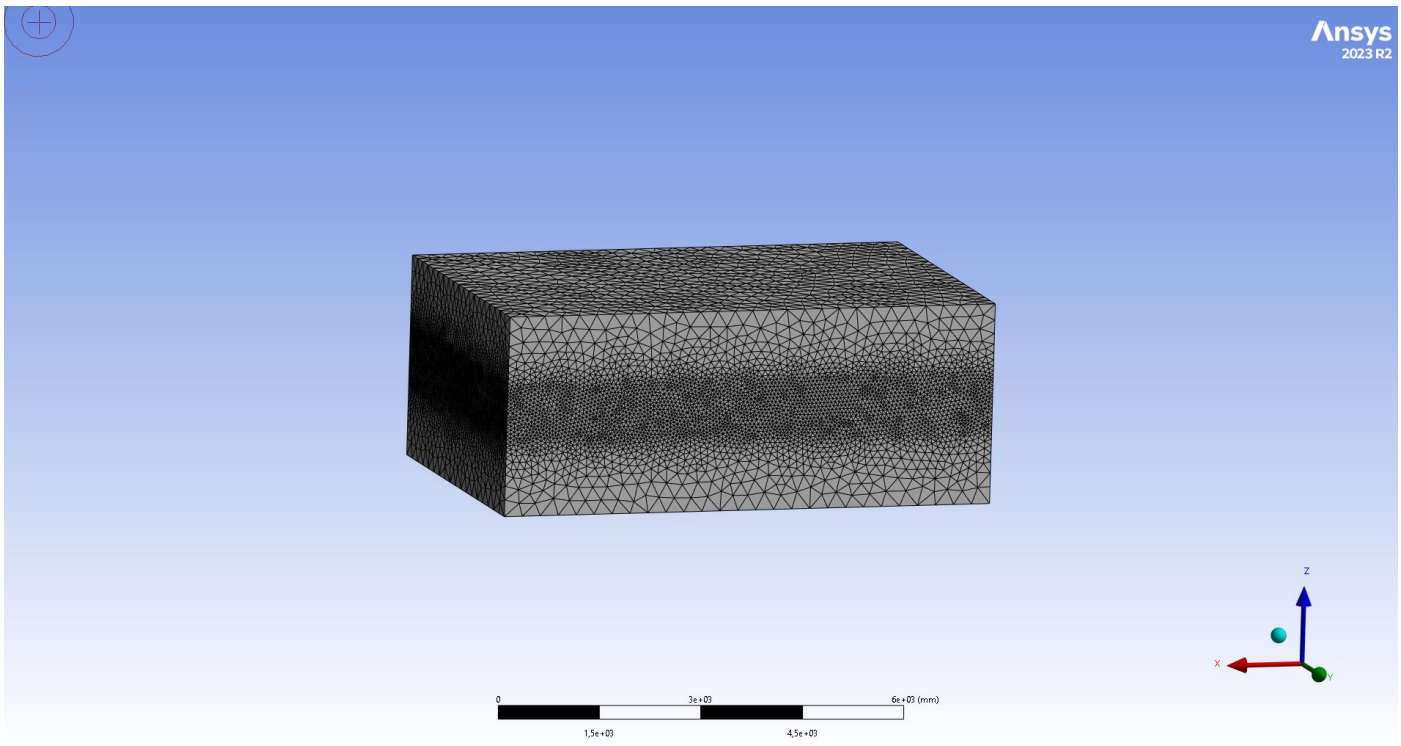


**Fig. C.4:** Cross-sectional view of the hybrid mesh structure, highlighting the refinement zone along the free surface for accurate VOF wave resolution.

Figure C.5 illustrates the detailed mesh topology surrounding the hull and the near-field region. Polyhedral elements were selected as the primary discretization type due to their superior ability to conform to complex hull geometries and their capacity to minimize numerical diffusion, thereby facilitating faster solution convergence compared to tetrahedral equivalents.

The dense stratification observed adjacent to the hull surface represents the boundary layer, where viscous effects and velocity gradients are most profound. These inflation layers were generated with a precise outward growth rate to maintain the dimensionless wall distance $(y^+)$within the range mandated by the turbulence model (k-omega SST). This configuration ensures the high-fidelity calculation of skin friction drag acting upon the hull by accurately resolving the near-wall flow physics.

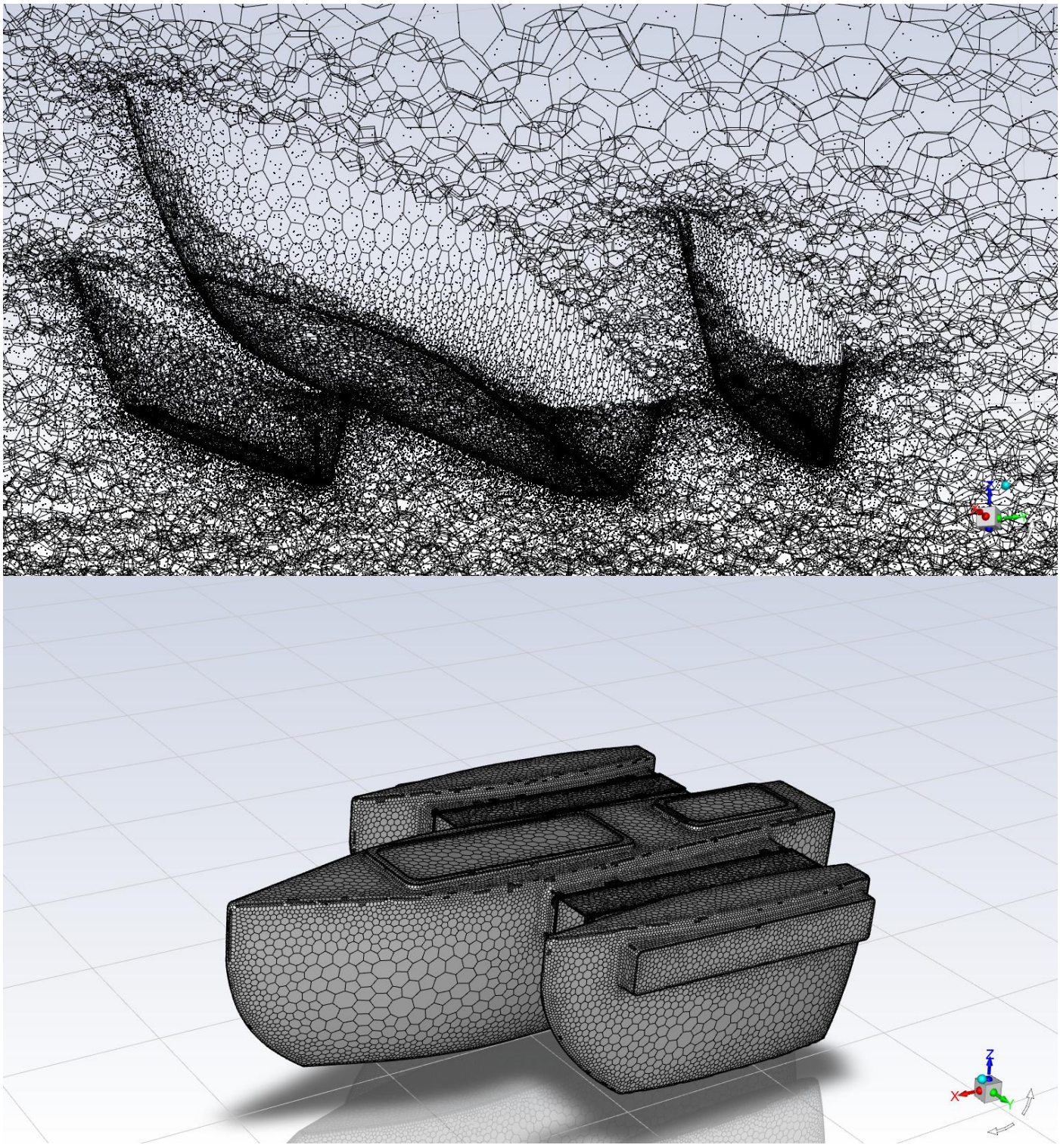


**Fig. C.5:** Close-up view of the hull surface mesh, demonstrating the polyhedral grid structure and the prism inflation layers generated for boundary layer capture.

### VOF (Volume of Fluid) Setup and Static Waterline

The Volume of Fluid (VOF) method was utilized to model the multiphase flow interactions. As depicted in the phase contour plot in Figure C.6, the computational domain is sharply divided based on volume fraction; the red region designates the water phase, while the blue region represents the air phase.

Prior to the initiation of dynamic simulations, the hull was initialized at the specific draft level corresponding to the designed full-load displacement, and static equilibrium was rigorously verified to ensure accurate buoyancy forces. Furthermore, for turbulence closure, the Shear Stress Transport (SST) k-omega model was selected as the governing equation set due to its superior accuracy in predicting flow separation and handling adverse pressure gradients near the hull walls.

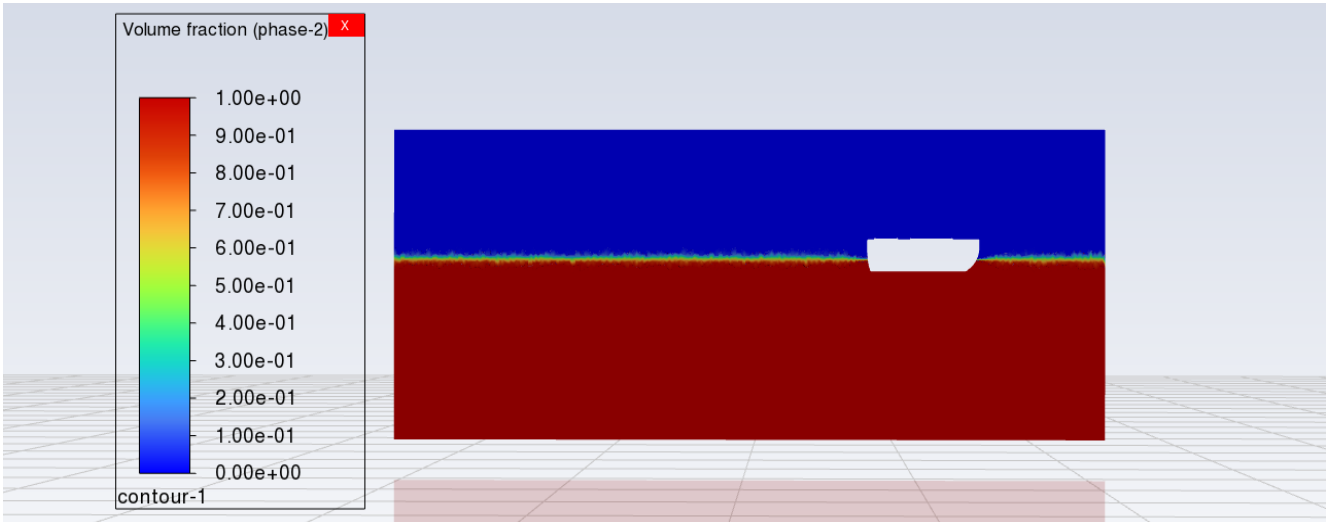


**Fig. C.6:** Volume fraction contours showing the initial static waterline setup; red indicates the water phase (Volume Fraction = 1) and blue indicates the air phase (Volume Fraction = 0).

### Free Surface Deformation and Wave Pattern Analysis

The free surface deformation and wave profile generated by the hull were analyzed at the designated operational cruising speed of approximately 3.9 knots (2 m/s). The post-processing results indicate that the characteristic wave system induced by the moving hull remains highly contained, with an observed average wavelength of 0.6 m and a peak wave amplitude limited to approximately 0.08 m.

As illustrated in Figure C.7, the bow wave formation exhibits significant minimization, a direct result of the optimized hull geometry. This low-amplitude wave profile is critical for operational safety, as it effectively prevents water spray from reaching the deck area. Furthermore, the wake structure trailing the vessel displays a coherent and regular pattern, demonstrating that the hull penetrates the water with minimal turbulent disturbance rather than generating excessive drag-inducing chaotic flow.

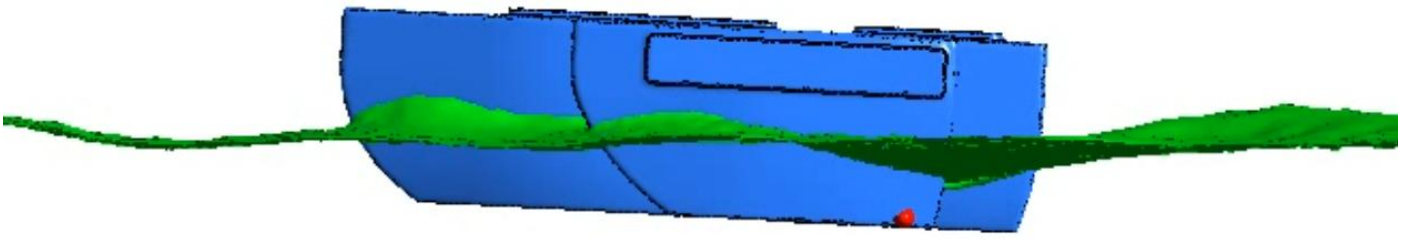

**Fig. C.7:** Free surface wave elevation contours at 2 m/s (3.9 knots) cruising speed, highlighting the minimized bow wave and regular wake pattern.

**Total Resistance and Drag Force Verification**

In the conducted Computational Fluid Dynamics (CFD) simulations, the time-dependent variation of hydrodynamic loads acting on the hull was monitored to evaluate resistance characteristics. As illustrated in Figure C.8, examination of the convergence history reveals that the transient oscillations observed in the initial phase of the simulation were effectively damped out, with the Total Drag Force reaching a steady-state regime at an average value of 40-42 N. This numerically verified resistance value served as the primary design input for the sizing of the vehicle's propulsion (thruster) system, ensuring that the selected motors provide sufficient thrust margin to overcome hydrodynamic resistance at the target cruising speed.

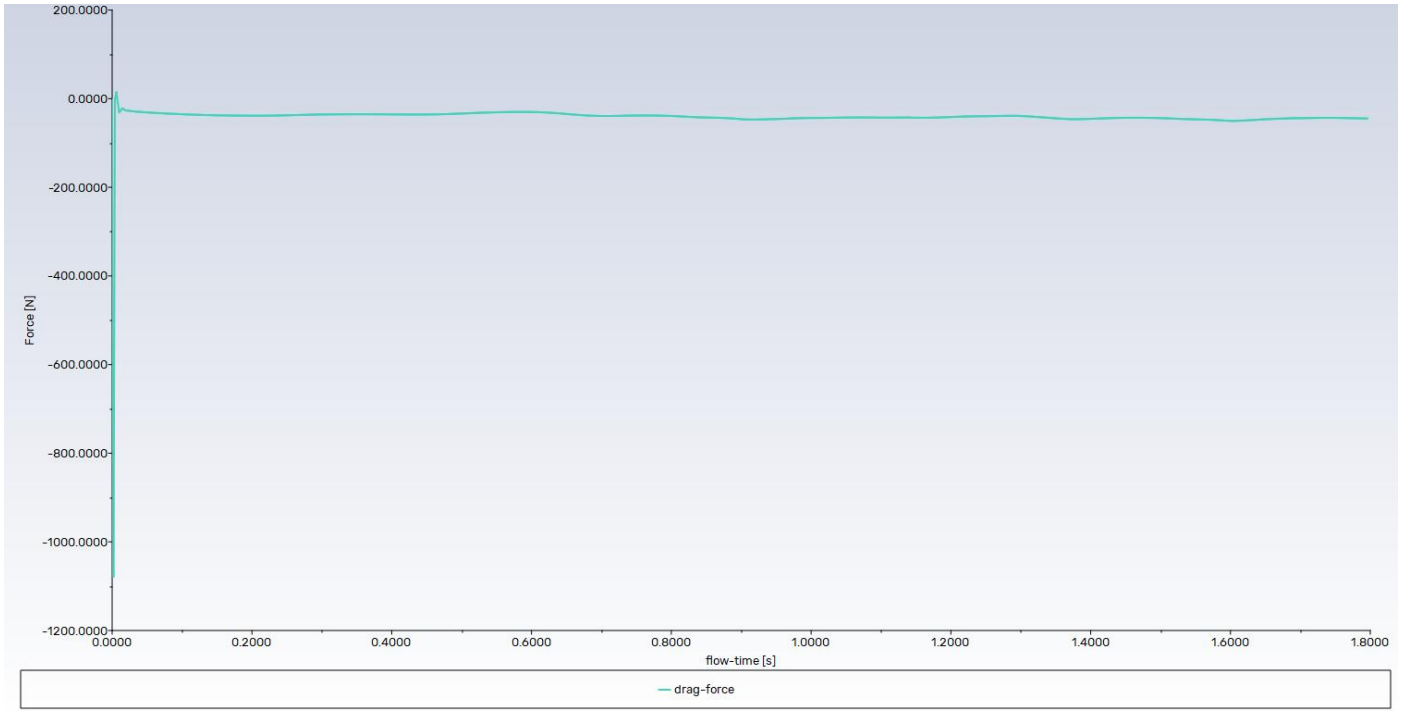


**Fig. C.8:** Time history of Total Drag Force convergence; the curve stabilizes at approximately 41 N, confirming the steady-state resistance load.

**Longitudinal Stability and Pitch Moment Analysis**

To validate the vehicle's longitudinal stability, the pitch moment acting on the hull was analyzed as a function of time. An examination of the data presented in Figure C.9 indicates that the initial moment oscillations were effectively damped, stabilizing within a negligible range of 0.033– 0.037, effectively converging to zero. This near-neutral moment balance demonstrates that the designed hull does not exhibit 'porpoising' instability at operational speeds and possesses a highly stable hydrodynamic profile.

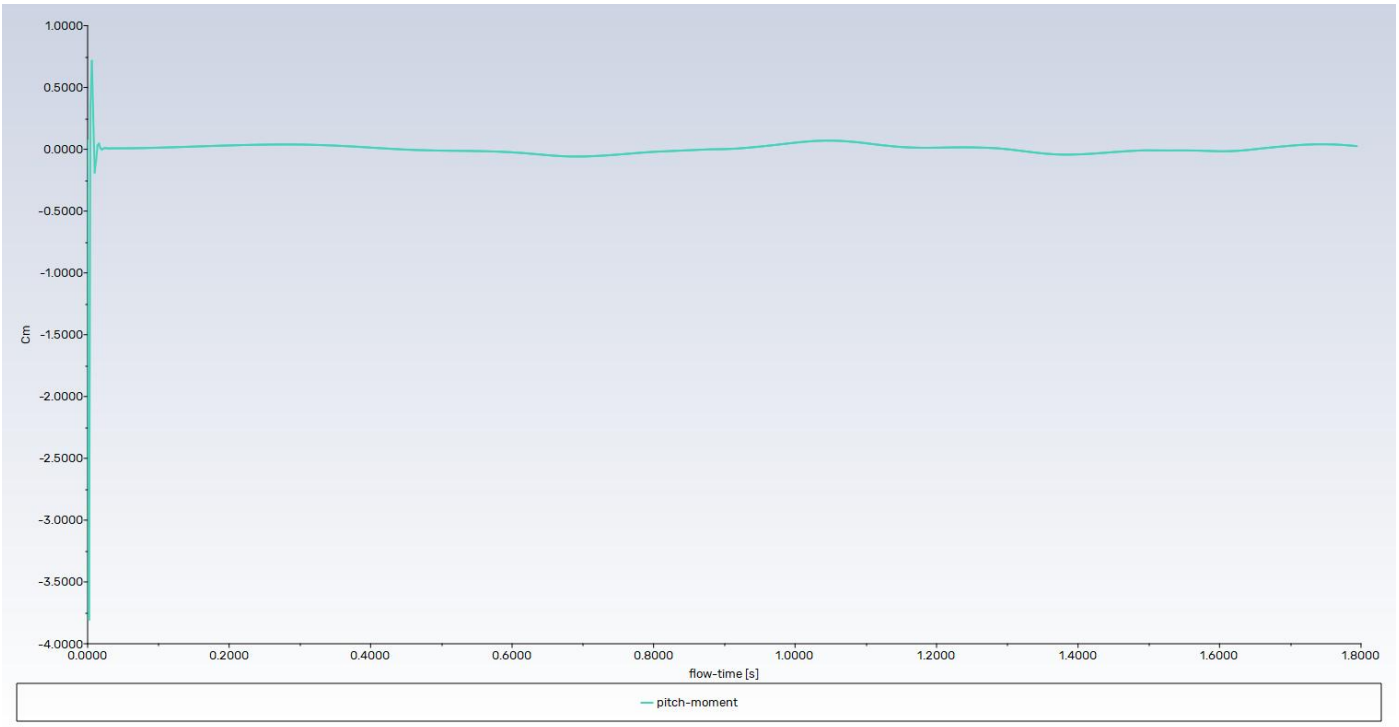


**Fig. C.9:** Temporal evolution of the Pitch Moment. The damping of oscillations indicates a stable equilibrium without excessive trim deviations.

**Heave Motion and Dynamic Equilibrium**

During the analysis process, the vertical motion (heave) of the hull was monitored under the 6-Degrees of Freedom (6-DOF) motion scheme. As clearly observed in the initial section of Figure C.10, the large-amplitude fluctuations represent the transient settling phase, where the vessel physically adjusts to the free surface to establish its natural waterline.

Following this initial stabilization period, these oscillations rapidly dampen out. Specifically, centering around the gravitational weight of approximately 245.25 N (corresponding to the 25 kg design mass), the hydrodynamic lift force was observed to oscillate within a narrow band between 240 N and 250 N before settling into a dynamic equilibrium. This result confirms that the interaction between the hull's buoyancy and the Center of Gravity (CoG) is modeled with high physical fidelity.

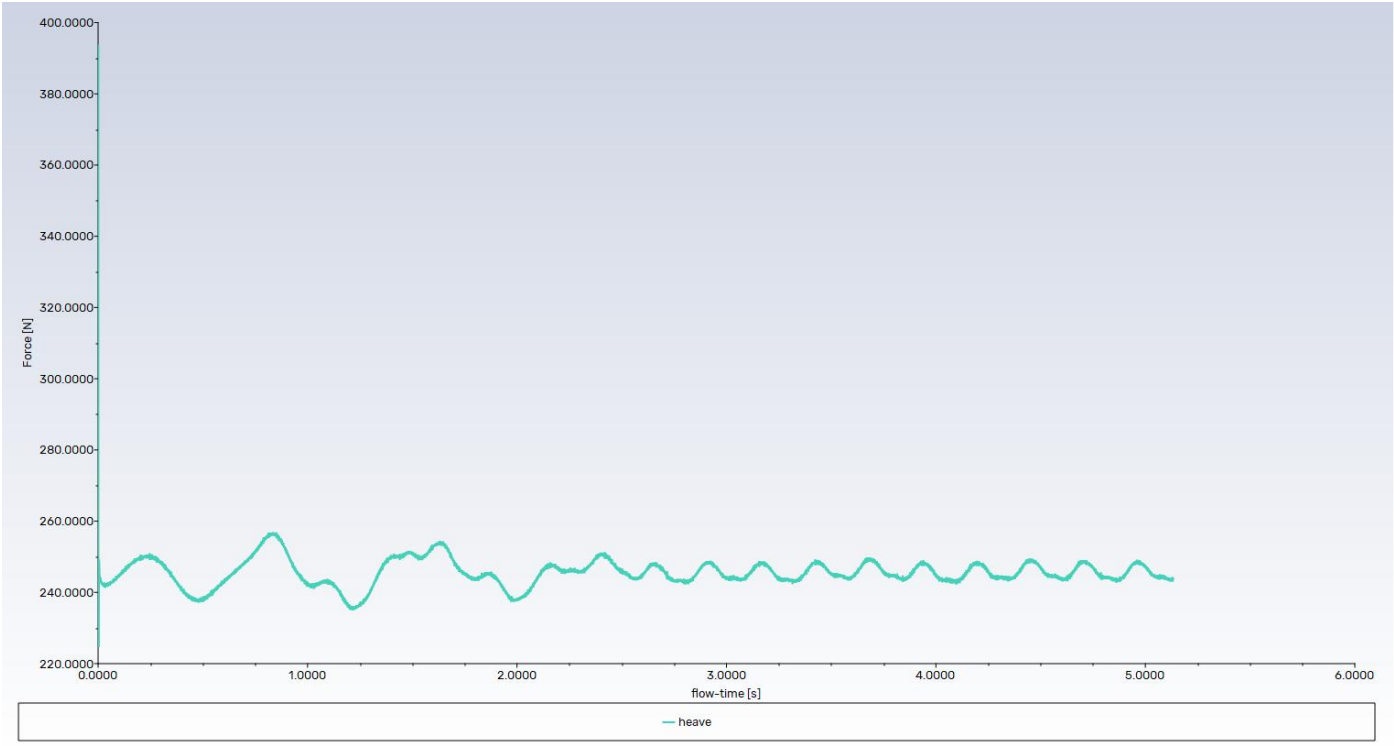


**Fig. C.10:** Heave response plot. The initial high-amplitude oscillations indicate the vessel's settling phase, which is followed by convergence to dynamic equilibrium around the gravitational weight (245.25 N).

APPENDIX D

## Electrical Subsystem Design Details

### *A. Design Methodology and Environment*

The electronic design strategy for the ASV prioritizes the Complexity vs. Reliability Trade-off. To maximize operational capabilities while minimizing failure probability, a Discrete Power Topology principle was adopted. All field tests were conducted in controlled environments: the inner harbor (boathouse) within the campus for environmental stability (wind/wave control) and a pool for precise sensor calibration.

Thermal performance analysis of the system is shown in Figure D.1.

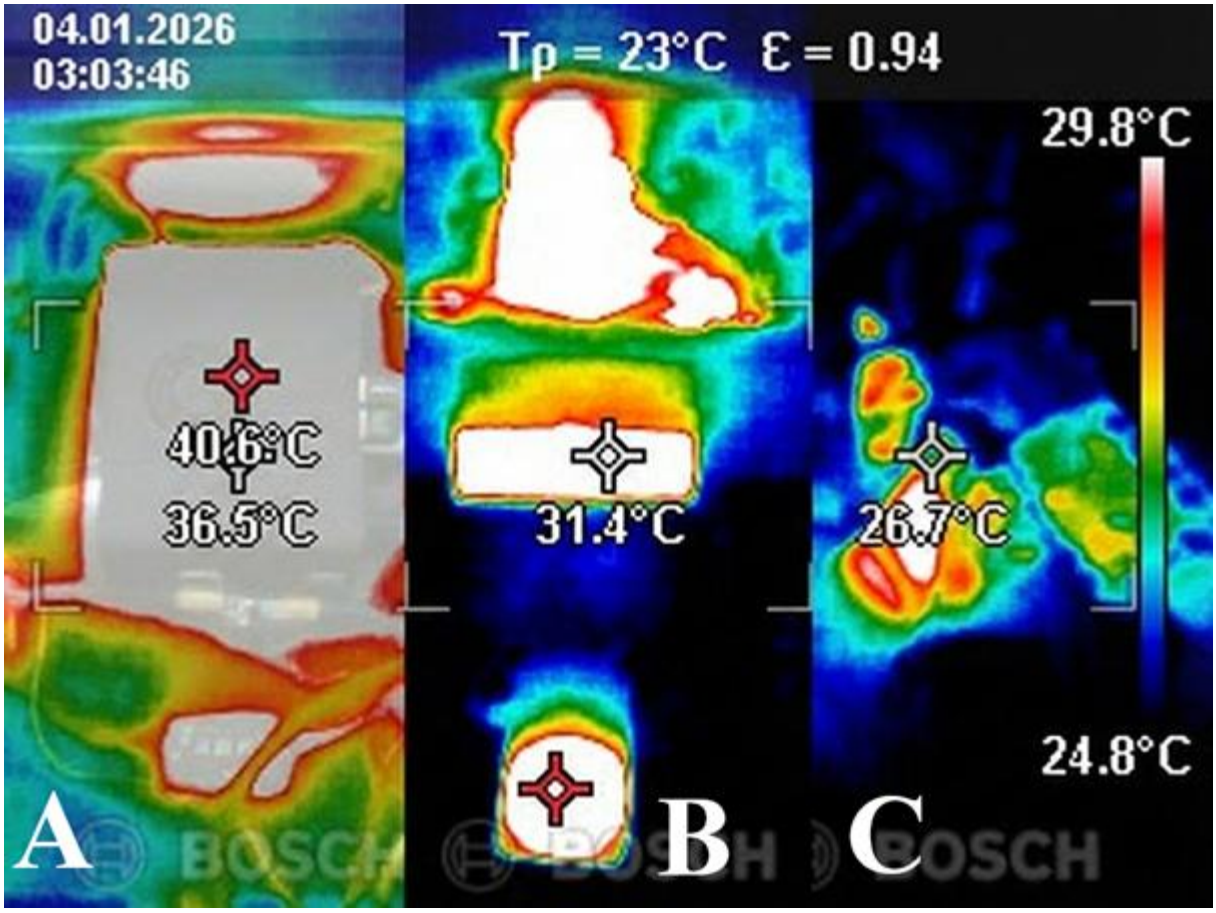


**Fig. D.1:** Thermal performance analysis under operational load conditions. Control Unit temperature stability (A), Navigation System heat dissipation (B), and Shooting System thermal response (C).

*B. Subsystem Design, Technical Implementation, and Verification*

*1) Power Architecture and Safety Infrastructure*

In line with safety and energy management procedures, a two-stage physical isolation mechanism was established. This includes a 200A Master Switch at the main energy input and a physical "Push-to-Stop" button on the hull for emergency intervention. The system's Fail-Safe architecture and electronic switching were shaped by engineering solutions developed to address technical failures observed in previous prototypes.

Mechanical contact relays (Finder series) used in past iterations were prone to corrosion from humidity and vibration in saltwater environments, creating a risk of contact welding due to electrical arcing. To eliminate this vulnerability, the design transitioned to Solid State Relay (SSR) technology, which utilizes a DC-DC control architecture without mechanical parts. A similar optimization was applied to the control logic; previous reliance on an external Arduino for emergency management caused language incompatibility (Python vs. C++) and increased complexity due to auxiliary power requirements. Consequently, the control mechanism was migrated directly to a secondary computer (NVIDIA Orin Nano).

However, since the Orin Nano's GPIO pins (3.3V LVTTL) and limited current capacity (~4mA) are insufficient to drive industrial SSRs, a 2N2222 NPN Bipolar Junction Transistor (BJT) was integrated into the signal line. Operating as a Logic Level Converter in Saturation Mode, this circuit allows the relays to be stably controlled via the main system without requiring an additional processor. Verification tests performed under active motor load (~20A) confirmed that the 2N2222-supported SSR circuit cuts the motor line with millisecond precision, protecting avionic systems and successfully executing the Fail-Safe procedure. The electronic switching and remote cut-off (Fail-Safe) architecture of the system is illustrated in Figure D.2. Furthermore, to prevent irreversible damage to the power boards caused by current spikes observed in previous tests, critical lines on the Matek Power Distribution Board (PDB) have been protected with 5A and 3A Fast-Blow AGC Glass Fuses suitable for the load characteristics.

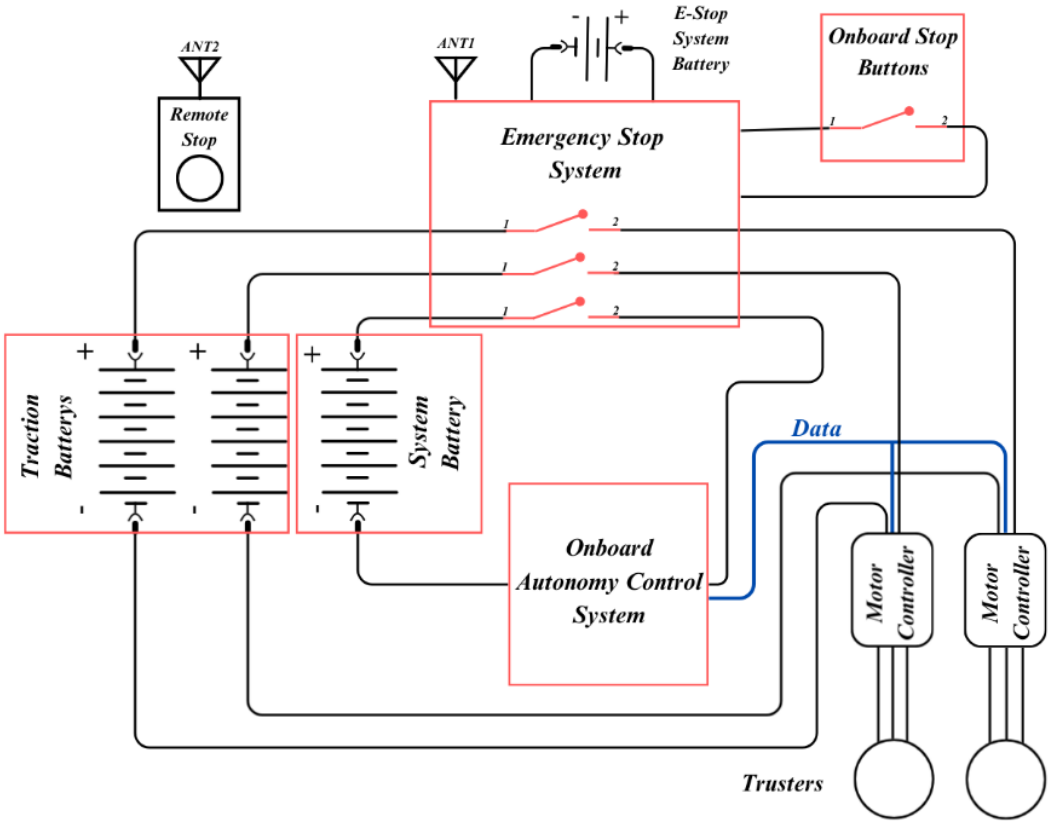


**Fig. D.2:** Electronic switching and remote cut-off (Fail-Safe) architecture of the system.

*2) Control Topology and Sensor Integration*

The vehicle's autonomous control architecture has been revised in line with hardware limitations encountered during field tests. Due to the insufficient coverage area of the ZED X Mini model initially used for visual perception, the ZED2i stereo camera with a 110° wide field of view (FOV) was integrated into the system. However, after observing that the standard model led to erroneous object detection due to susceptibility to sun reflections (Specular Reflection) on the water surface, the hardware was updated to the ZED 2i model featuring a built-in Polarizing Filter, thereby eliminating optical noise.

Similarly, the Inertial Measurement Unit (IMU) data flow, initially planned via the Pixhawk Orange Cube, was revised after reports indicated that the ZED2i camera's internal sensor (800Hz sampling rate) operates much more synchronously with visual odometry data and with a significantly lower noise ratio; consequently, the camera sensors were selected as the primary source for orientation.

For acoustic signal processing tasks, the Deity V-Mic D3 Pro microphone, featuring a Super-Cardioid polar pattern, was chosen to better isolate ambient noise. Thanks to its built-in stepless gain control, this hardware boosts the signal level at the source, increasing the SNR (Signal-to-Noise Ratio), and ensures clean data acquisition even in windy harbor conditions via the Deadcat (Windshield) attachment. The sensor is digitized via a USB sound card over a 3.5mm analog interface and integrated into the NVIDIA Jetson AGX Orin.

For environmental mapping, the system transitioned to the RPLiDAR S3 model. Since the rear field of view of this sensor—which transmits data via high-speed serial communication (USB/UART)—is occluded by the vehicle's body structure, the scanning angle was software-limited to 270 degrees instead of 360, thus eliminating unnecessary data processing load. Regarding positioning, the sufficiency of the HerePro GPS module's Stand-Alone mode was verified, and operational efficiency was enhanced at a 10Hz update rate by avoiding the installation complexity of the RTK mode. The design of the electronics suite is illustrated in Figure D.3.

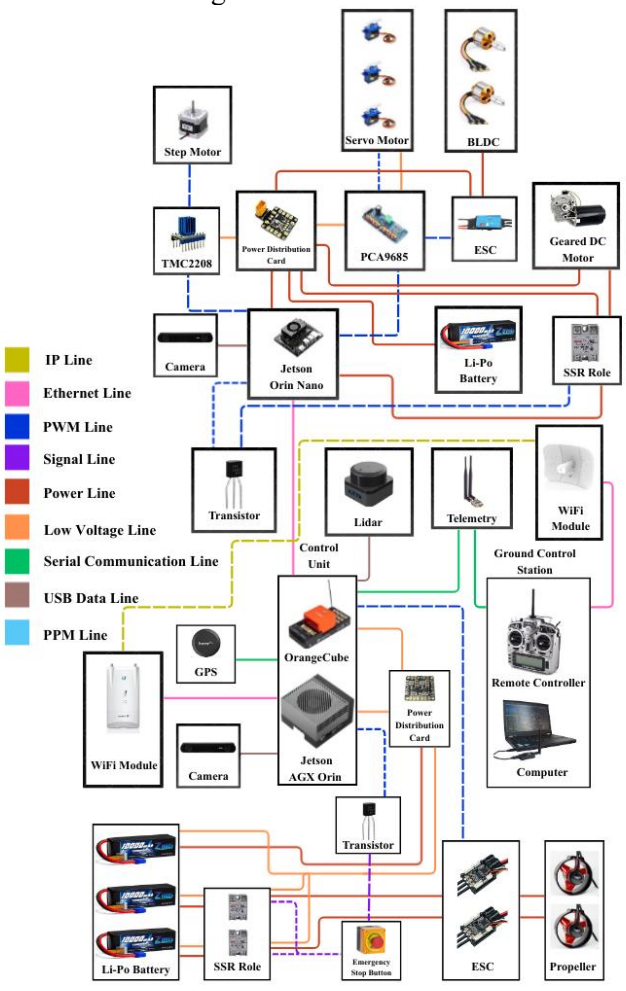


**Fig. D.3:** Comprehensive architecture of the vehicle's electronics suite, including sensor integration, communication interfaces, and actuator control lines.

*3) Communication Infrastructure*

The communication architecture has been fortified by analyzing competition experiences gained in previous years and communication breakdowns encountered during inner harbor tests. RFD series long-range modules, utilizing Frequency Hopping Spread Spectrum (FHSS) technology and communicating via the UART protocol, were integrated into the system. Field tests confirmed that the RFD modules maintained continuous data flow. Since this RF link is dedicated solely to transmitting small-sized data packets—specifically ASV navigation telemetry and GCS state-change commands—it was deemed exempt from high-speed throughput testing.

Conversely, regarding the video transmission line, it was observed that the Ubiquiti Rocket M5 hardware used on both the Ground Station and Vehicle sides in last year's competition was insufficient to meet increasing data load and range requirements. To overcome this performance constraint, the onboard M5 unit was retained, while the Ground Station (Base) hardware was upgraded to the Ubiquiti LiteBeam AC Gen2 (LBE-5AC-Gen2) system, which operates on the 5GHz 802.11ac standard and offers 23dBi high gain with focused signal power. Given that this Wi-Fi link handles large-volume data transmission, it was subjected to rigorous speed testing. The field range test results of this hybrid integration (Rocket M5 ↔ LiteBeam AC) are presented in Figure D.4 and Figure D.5:

- **Limit Condition Test (Figure D.4):** In scenarios where the vehicle pushed range limits or faced physical obstructions, it was observed that although signal power dropped to a critical level of -91 dBm, the connection remained stable and video streaming was sustainable.
- **Nominal Operation Test (Figure D.5):** In tests conducted within the standard operational zone, the signal power stabilized at -47 dBm thanks to the new antenna's high gain. Furthermore, data throughput exceeded 100 Mbps, ensuring low-latency and high-resolution video transmission.

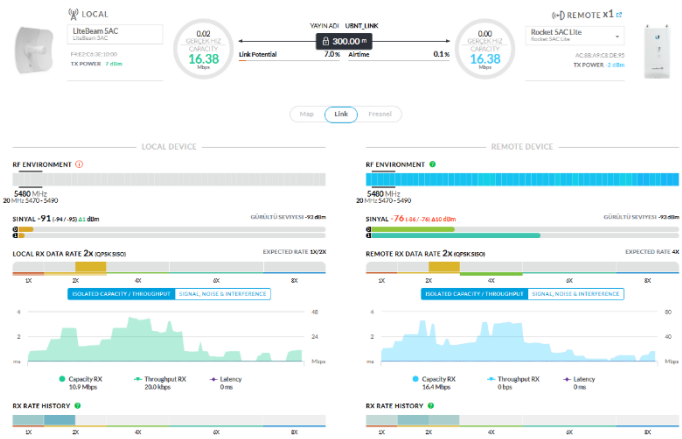

**Fig. D.4:** Signal stability under limit conditions (-91 dBm)

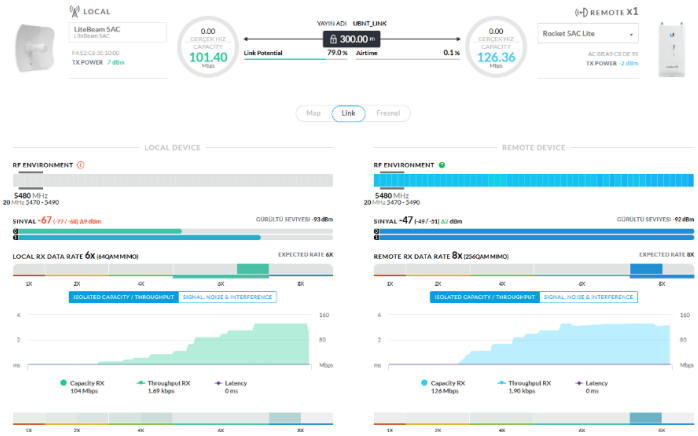

**Fig. D.5:** High-throughput performance (>100 Mbps) during nominal operation.

*4) Propulsion System and Motor Drivers (Performance Analysis)*

The propulsion system is built upon two Degz Ultras brushless DC (BLDC) motors, distinguished by their hydrodynamic efficiency. During the initial integration phase, it was determined that the 4S battery configuration limited the motor torque capacity; consequently, the system voltage was revised, and a transition to a 7S (25.9V Nominal) battery infrastructure was made to achieve maximum efficiency.

Regarding driver technology, tests revealed that the standard bidirectional underwater ESCs used initially caused synchronization loss, mechanical stuttering, and acoustic noise during sudden maneuvers. To eliminate these risks, motor control was delegated to Flipsky VESC 6.7 70A electronic speed controllers communicating via UART. In Sensorless commutation mode, the electrical characteristics of the motors were analyzed using the Field Oriented Control (FOC) interface to ensure optimal calibration. In full-load tests (~1200W Peak Power) conducted with the 7S battery configuration and during sudden directional changes, it was verified that the VESC drivers operated synchronously, and that mechanical stuttering, noise, and vibration issues were completely eliminated thanks to the FOC settings. Data pertaining to the propulsion system is presented in Figure D.6.

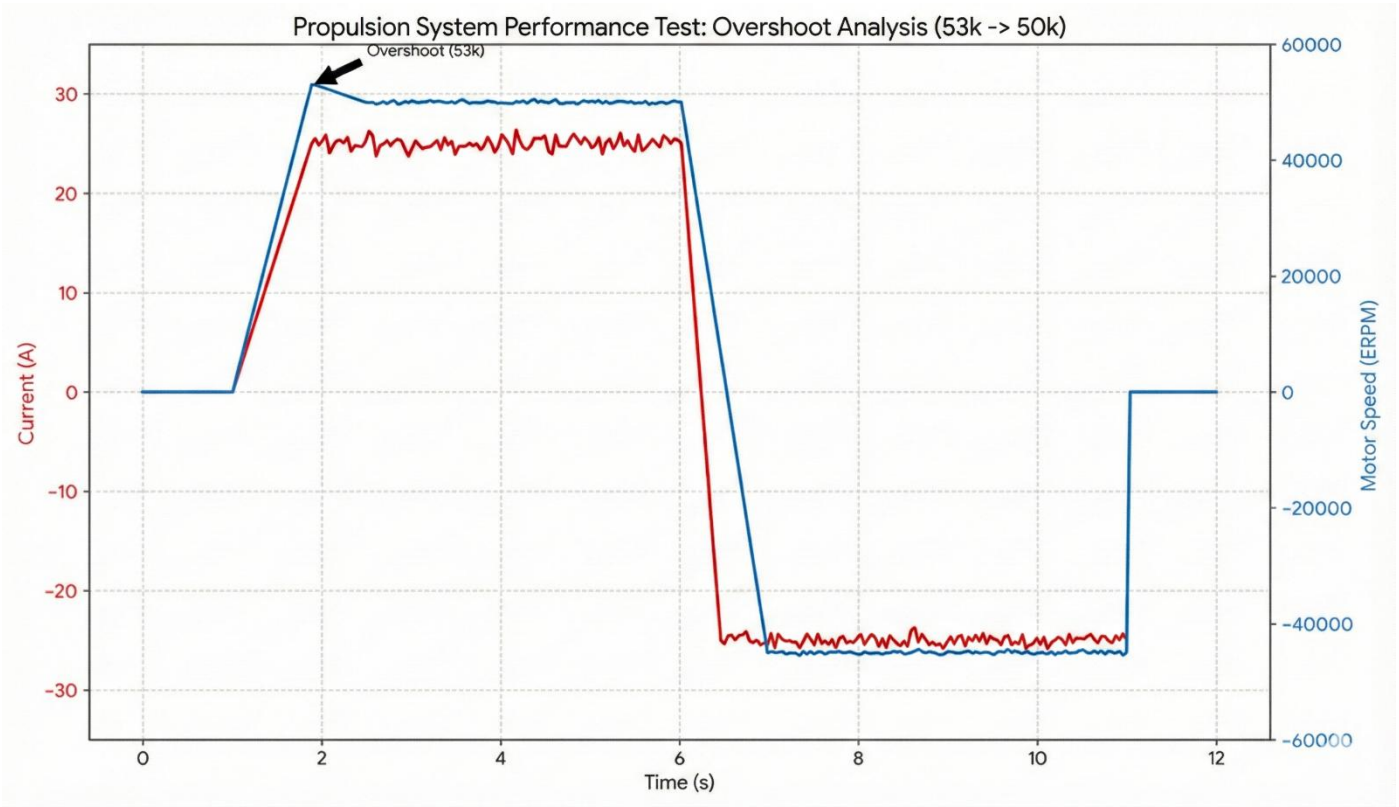


**Fig. D.5:** Propulsion System High-RPM Dynamic Load Test (X-Y Analysis).

*5) Payload and Integrated Firing System*

The payload features a creative and hybrid design that overcomes mechanical constraints. The system was redesigned because the rotary conical magazine structure driven by a 28BYJ-48 stepper motor used in the previous prototype produced low torque and created lateral (yaw) maneuver limitations; consequently, the complex rotating structure was replaced by a gravity-fed linear tube magazine system. This new system is built upon a Racquetball Delivery Module driven by a NEMA 17 stepper motor with a 1.8° step angle and a TMC2208 driver operating in UART mode, which features silent drive technology. By eliminating the need for an external microcontroller (Arduino), the system has been made directly manageable via the NVIDIA Orin Nano, and an external ZED 2i camera has been mounted on the module for target detection.

The water firing system is driven by a 12V DC Bosch TMS 41210030081 (0986337402) wiper motor, chosen for its high torque capacity and durability. The motor is triggered via an SSR (Solid State Relay) mechanism powered by the Matek PDB 12V line, while the Orin Nano's GPIO signal is controlled after being amplified by a 2N2222 transistor circuit. During integration tests involving the sequential triggering of the Racquetball module and the water motor, it was verified that the Orin Nano remained protected thanks to the transistor circuit, and all actuators operated stably. The electronic schematic of the firing system is shown in Figure D.6.

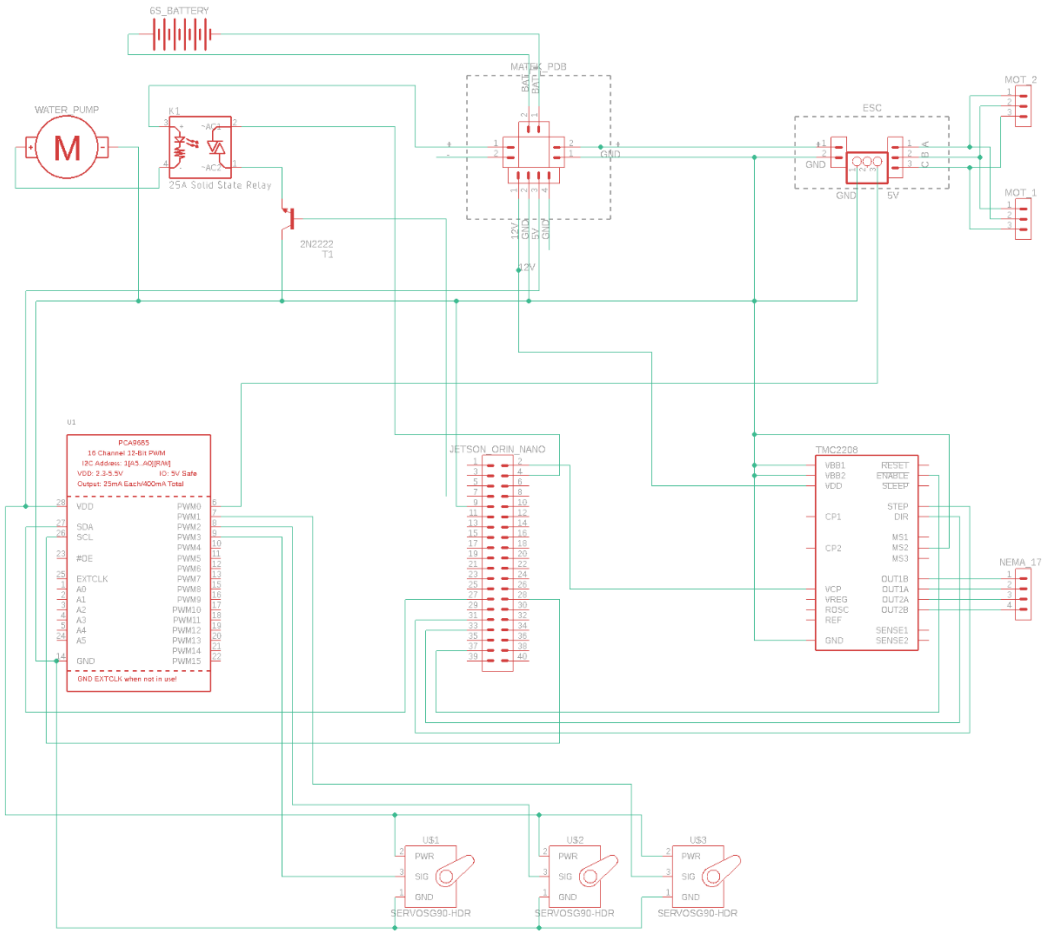


**Fig. D.6:** Electronic schematic of the firing system.

*6) Energy Efficiency, Electromagnetic Compatibility (EMC), and Grounding*

To prevent cable clutter and signal interference, a Star Grounding topology has been implemented; all ground lines (GND) are gathered at a single common reference point on the Matek PDB, thereby minimizing potential failure points. High-noise lines, such as motor cables, and I2C/UART data lines have been routed through physically separate channels. Specifically, signal integrity has been safeguarded in GPS and Compass lines using Twisted Pair structures and Ferrite Beads.

In the system's Power Budget analysis, the avionics backbone has been upgraded to a dual-computer architecture comprising the NVIDIA Jetson AGX Orin (Main, Avg. 2.6A) and Orin Nano (Secondary, Avg. 1.2A). Along with the ZED 2i, HerePro GNSS, and Pixhawk controller, the baseline energy consumption has been optimized. Regarding dynamic loads, the propulsion system draws an average of 18.0A at nominal cruising speed. When the lateral movement system and communication modules are included, the vehicle's total current consumption is recorded as approximately ~25.6A on average, and ~36.4A under maximum load. Based on this data, operational mission time has been maximized with a 7S (22.2V) battery configuration. The power consumption table is shown in Table D.1.

**Table. D.1:** System Power Budget Analysis.

| Component Group | Hardware Component | Operating Voltage | Max Current (Peak) | Avg. Current (Nominal) | Power Source |
|---|---|---|---|---|---|
| Propulsion System | 2 x Degz Ultras Motor | 25.9V | 25.0 A | 18.0 A | Main Battery (Direct) |
| Main Computer | NVIDIA Jetson AGX Orin | 19V | 3.16 A (60W) | 2.6 A (50W) | 19V Regulator |
| Secondary Computer | NVIDIA Jetson Orin Nano | 12V | 2.08 A (25W) | 1.25 A (15W) | 12V Regulator |
| Motor Control | Pixhawk Orange Cube | 5V | 1.0 A | 0.5 A | Matek PDB (5V BEC) |
| Sensors | ZED 2i + HerePro GPS | 5V | 2.5 A | 1.8 A | Orin USB / 5V BEC |
| Communication | Ubiquiti Module | 24V | 0.65 A | 0.4 A | 24V Regulator |
| Lateral Movement | NEMA 17 + Servos | 12V / 5V | 2.0 A | 1.0 A | PDB (12V Line) |
| **TOTAL** | **Whole System** | **-** | **~36.4 A** | **~25.6 A** | **12.8Ah Li-ion** |

Calculation Summary:

- **Battery Capacity:** 12,800 mAh (12.8Ah)
- **Theoretical Operation Time (Cruising):** (12.8Ah / 25.6A) * 60 min ≈ 30 Minutes
- **Safety Margin:** With a 20% reserve, a safe mission time of ~24 Minutes has been verified.

APPENDIX E

## System Flow Diagram

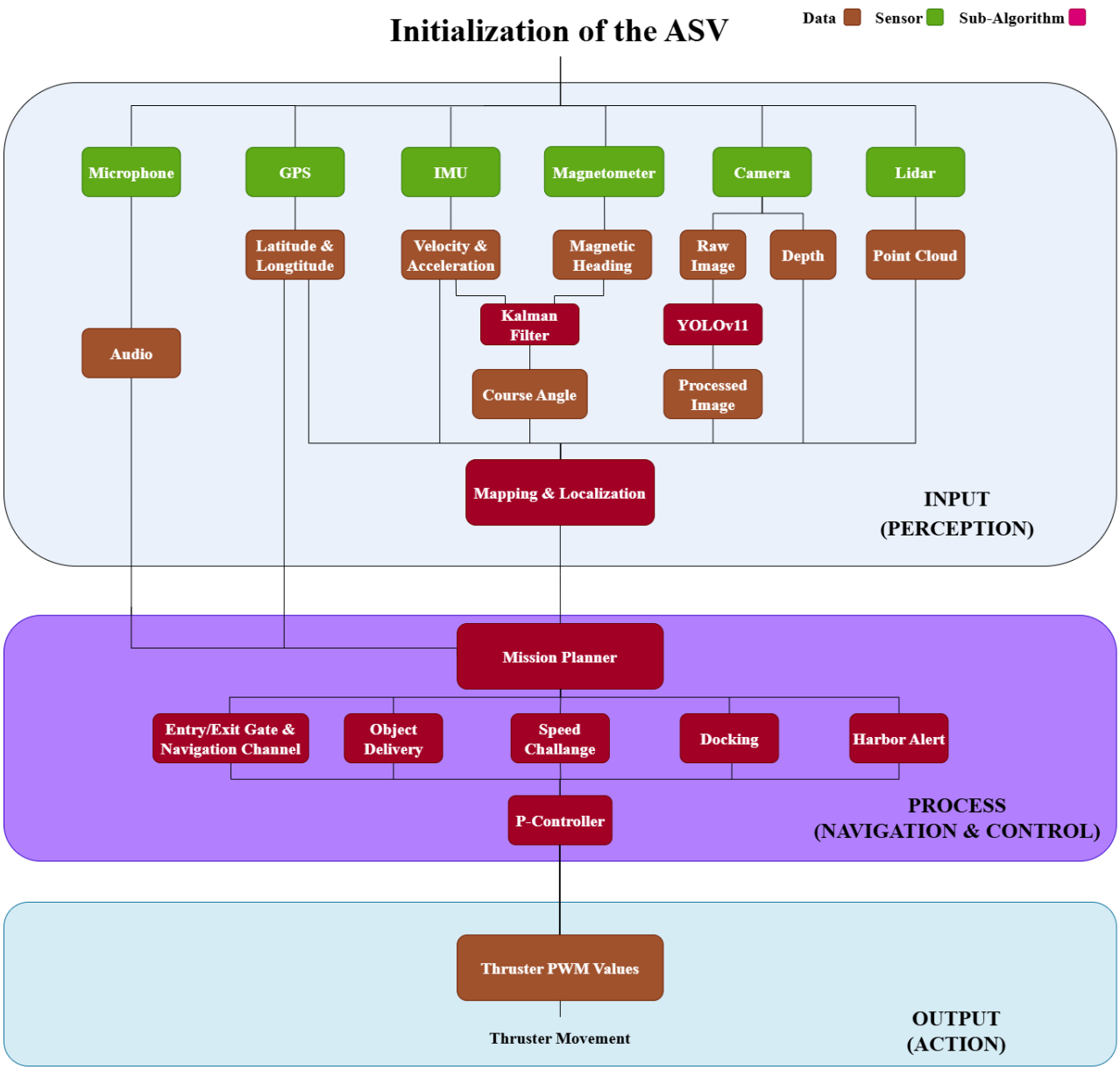


**Fig. E.1:** System Flow Diagram of the ASV illustrating the data flow across Perception, Navigation, and Action layers.

APPENDIX F

## Team BlueHomeland Gantt Chart

**Table C.1:** Work Breakdown Structure and Proposed Timeline

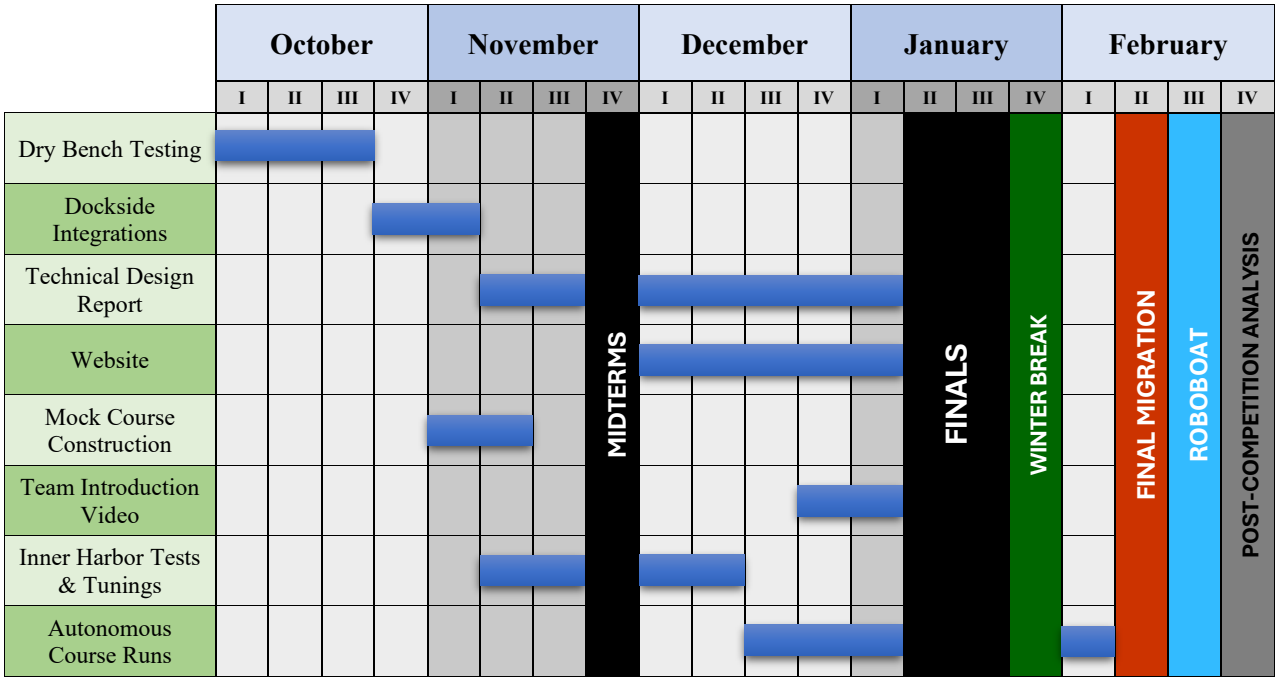

APPENDIX G

## Test Plan and Results

**Table D.1:** Comprehensive System Verification and Validation (V&V) Matrix

| Test ID | Category | Test Description | Environment / Method | Succes Criteria | Result | Status | Test Date |
|---|---|---|---|---|---|---|---|
| T-SIM-01 | Simulation | Hydrodynamic Drag & Stability (ANSYS) | CFD Analysis: Flow analysis in ANSYS Fluent at various speeds (1m/s, 2m/s). | Drag Coefficient (Cd) < 0.6 | Cd: 0.45 | Pass | 06.10.2025 |
| T-SIM-02 | Simulation | Virtual Maneuver & Buoyancy | Fluent: Weight distribution and floatation test in virtual environment. | Waterline must match reference level; no virtual sinking. | Waterline 1 cm below ref (Acceptable). | Pass | 09.10.2025 |
| T-MEC-01 | Mechanical | CoG Verification | Lab Bench: 3-axis balance test by suspending the vehicle. | CoG must be below the Geometric Center and centered. | Batteries shifted 2 cm forward to align CoG. | Pass | 10.10.2025 |
| T-MEC-02 | Mechanical | Static Waterproofing | Pool: Vehicle submerged (sealed) for 60 minutes. | 0 ml water ingress inside the hull. | Waterproofing verified. | Pass | 13.10.2025 |
| T-MEC-03 | Mechanical | Dynamic Float & Swim | Pool: Manually controlling the ASV | Smooth cruising profile with minimal pitch (pitch < 5°) and no nose-diving. | Observed stable swimming. | Pass | 14.10.2025 |
| T-MEC-04 | Mechanical | Object Delivery Module Accuracy | Land: Shooting target from 3m distance. | 7/10 hits minimum and water reach the target. | 8/10 hits and water contact confirmed | Pass | 17.10.2025 |
| T-ELE-01 | Electronics | System Power Consumption | Bench: All systems active (Jetson, Sensors, Thrusters). | Total current draw < 50A (PDB Limit). | Avg: 34A, Peak: 48A. | Pass | 18.10.2025 |
| T-ELE-02 | Electronics | Shooter System Voltage/Amp | Bench: Measurement during shooter mechanism trigger. | Voltage Sag must be < 0.8V. (Jetson shutdown threshold for GPIO pins is 4.2V) | Instant drop 0.3V, no system reset. | Pass | 19.10.2025 |
| T-ELE-03 | Electronics | 7S Battery & Thruster Upgrade | Pool: Transition to 7S battery and thrust measurement. | Thrust > 11.27 kgf/motor, ESC Temp < 60°C. | Thrust: 13.1 kgf ESC Temp < 46 °C. | Pass | 20.10.2025 |
| T-ELE-04 | Electronics | Signal Interference (EMI) | Bench: Sensor data check while motors at full throttle. | No data loss or signal corruption allowed. | Magnetic heading from ZED2i is unstable. Bigger gap between ASV and camera solved the problem. | Pass | 20.10.2025 |
| T-HRD-01 | Hardware | Sensor Configurations (ZED, Lidar, IMU) | Drivers: Sensor initialization and FPS/Hz check. | ZED: 30fps, Lidar: 10Hz, IMU: 100Hz stable. | All sensors running in parallel confirmed. | Pass | 20.10.2025 |
| T-HRD-02 | Hardware | OrangeCube & GPS Setup | MissionPlanner: Satellite number and HDOP value check | Satellites > 12, HDOP < 1.0. | Satellites: 20, HDOP: 0.5. | Pass | 21.10.2025 |
| T-SOF-01 | Software | AGX Orin Libs & Requirements | AGX Orin: JetPack 6.1, CUDA, PyTorch, TensorRT compatibility check. | Libraries must run without conflict. | TensorRT version mismatch resolved. | Pass | 24.10.2025 |
| T-SOF-02 | Software | Audio Band-Pass Filtering | Bench: Injecting noise and target signal (sine wave) into the filtering algorithm. | Only 600-1200Hz range must pass; outside frequencies must be attenuated. | 1kHz tone detected; noise successfully filtered. | Pass | 26.10.2025 |
| T-SOF-03 | Software | GCS Map Integration & UI Upgrade | Bench: Integrating high-res offline maps of Sarasota/Nathan Benderson Park and adding macro keys. | Map renders with zero lag; New functional keys must trigger the ASV side. | Sarasota map cached & zoomable. Six new shortcut keys active. | Pass | 28.10.2025 |

| | | | | | | | |
|---|---|---|---|---|---|---|---|
| T-COM-01 | Comms | GCS Telemetry & UDP Bridge | Field: Bi-directional data stream test. | Latency < 1000ms, Packet Loss < 1%. | Latency 45ms(UDP)-700ms(RF) stream stable. | Pass | 01.11.2025 |
| T-COM-02 | Comms | Remote Mode Switching (Manual-Auto) | Dockside: Toggling mode via GCS UI and monitoring ASV mode flag seen on toggle. | ASV state must update within < 2000ms; mode flag signal received by GCS. | Transition observed (1000ms); ASV mode flag on GCS confirmed change. | Pass | 04.11.2025 |
| T-SAF-01 | Safety | Fail-Safe (Physical & RF) | Dockside: E-Stop button and RC kill-switch test. | Motors must stop instantly (0 sec). | E-Stop button cuts the power to thrusters. RF Loss triggers "Hold Mode". | Pass | 05.11.2025 |
| T-SAF-02 | Safety | Tow Point Structural Test | Dockside: Applying static tension to the rear tow eyelet/hook. | No hull deformation or cracking; Tow point must be easily accessible. | Withstood tension test, accessibility confirmed. | Pass | 08.11.2025 |
| T-CTR-01 | Control | RC Manual Drive | Inner Harbor: Manual driving and maneuverability check. | Instant response to commands, no deadzone issues. | Control sensitivity verified. | Pass | 08.11.2025 |
| T-CTR-02 | Control | P-Controller Tuning (Mule) | Inner Harbor: Tuning PID on the test boat (Mule). | Minimal oscillation during heading hold. | P-Gain optimized for Mule dynamics. | Pass | 11.11.2025 |
| T-AUT-01 | Autonomy/ Navigation | Magnetic Heading Calibration | Dockside: ZED2i Heading vs. True North verification. | Error < 7° after magnetometer calibration and declination adjustment. | Error is 4-5° after recalibrations and declination adjustment. | Pass | 11.11.2025 |
| T-AUT-02 | Autonomy/ Navigation | Single Waypoint Arrival | Inner Harbor: Navigate to a single GPS coordinate. | Acceptance Radius < 2 m. | Reached 1-1.5 m from target. | Pass | 13.11.2025 |
| T-AUT-03 | Autonomy/ Navigation | Multi-Waypoint Path Following | Inner Harbor: Zigzag path following task. | Cross-Track Error (XTE) < 1.5 m. | Avg XTE: 0.8 meters. | Pass | 14.11.2025 |
| T-AUT-04 | Autonomy/ Navigation | Station Keeping (Position Hold) | Inner Harbor: Hold position under wind/current. | Drift < 3 m radius for 60 seconds. | Held within 3 m radius. | Pass | 17.11.2025 |
| T-AUT-05 | Autonomy/ Perception | Simultaneous Mapping & Localization (SLAM) | Inner Harbor: Mapping the course area. | Loop closure consistency required. | Localization drift < 0.5m based on GPS accuracy. | Pass | 24.11.2025 |
| T-AUT-06 | Autonomy/ Perception | YOLOv11 & Lidar Accuracy | Inner Harbor: Detection of objects at known distances. | Class Accuracy > 70%, Distance Error < 30 cm. | Buoy detected (75%), Distance Error: 10 cm. | Pass | 24.11.2025 |
| T-AUT-07 | Autonomy/ Navigation | Path Planning (A* algorithm) | Inner Harbor: Generating path avoiding obstacles. | Collision-free shortest path generation. | A* generates path in < 0.2 s. | Pass | 07.12.2025 |
| T-AUT-08 | Autonomy | Dynamic Obstacle Avoidance | Inner Harbor: Cruising through random buoys placed on the path. | No collision, Maintain safety distance. | Rerouting successful, safe pass. | Pass | 09.12.2025 |
| T-AUT-09 | Autonomy | Orbit / Circle Maneuver | Inner Harbor: Orbit around a GPS point. | Safety Distance to target > 1 m, full 360° loop. | 2 full loops, Avg Distance to target: 2.5 m. | Pass | 13.12.2025 |
| T-AUT-10 | Autonomy/ Logic | Task Preemption & Resume | Inner Harbor: "Delivery" task injected during navigation. | Pause task -> Deliver -> Resume from last state. | Resumed path to WP-2 after delivery. | Pass | 15.12.2025 |
| T-AUT-11 | Autonomy/ Perception | Target Geolocation Estimation | Inner Harbor: Calculating GPS coordinates of a target. | Geolocation Error (CEP) < 2 m. | Avg Error: 1.8 m. | Pass | 16.12.2025 |
| T-SYS-01 | System | Sea Maneuverability | Inner Harbor: Autonomous maneuver in strong wind and waves. | Heading stability in waves/wind. | Stable in wind/waves conditions. | Pass | 17.12.2025 |
| T-SYS-02 | System | Cold Start Time (Boot-to-Mission) | Dockside: Time from Power-On to "Auto Ready". | Total time < 60 seconds. | Boot sequence: 48 seconds. | Pass | 17.12.2025 |

| | | | | | | | |
|---|---|---|---|---|---|---|---|
| T-AUT-12 | Autonomy | Confined Space Docking (U-Turn) | Inner Harbor: Entering narrow dock, reversing out. | No contact, Wall-following on exit. | Mock dock prepared, tests are ongoing to reach success criteria | In Progress | 19.12.2025 |
| T-AUT-13 | Autonomy/ Full | End-to-End Autonomous Run | Inner Harbor: Complete run (Obstacle avoidance-> Delivery -> Speed Challenge -> Sound Signal -> Docking). | Completion < 15 minutes, No user interaction. | Mock course prepared, sequential tests are ongoing without docking. | In Progress | 21.12.2025 |
| T-MIG-01 | Migration | Mule to Final Hull Migration | Bench: Transfer electronics & thrusters to Final Hull. | Secure mounting, clean cable management. | Planned and scheduled. | Scheduled | 05.02.2026 |
| T-SYS-03 | System | Final Hull Maiden Voyage | Inner Harbor: First float & RC test of the Final Hull. | Correct waterline, no leaks, stability and sensors check. | Planned and scheduled. | Scheduled | 07.02.2026 |
| T-CTR-03 | Control | Final PID Tuning (New Dynamics) | Inner Harbor: Retuning Controller for Final Hull mass/drag. | Compensation for inertia change. | Planned and scheduled | Scheduled | 08.02.2026 |
| T-AUT-14 | Autonomy/ Full | Post-Migration Autonomous Run | Inner Harbor: Complete run with Final Hull. | Verify software/hardware sync on new body. | Planned and scheduled | Scheduled | 10.02.2026 |
| T-AUT-15 | Autonomy/ IVC | Inter-Vehicle Communication (IVC) link | Inner Harbor: GPS/Heading data packet transfer between Mule and Final boat via RF modules. | Packet Loss < 1%, Latency < 200ms. | Planned and scheduled | Scheduled | 12.02.2026 |
| T-AUT-16 | Autonomy/ IVC | Leader-Follower Tracking | Inner Harbor: 'Mule' boat executes autonomous run as 'Leader'; 'Final' boat autonomously tracks it. | Maintain tracking distance (5 m); Deviation < 1.5 m. | Planned and scheduled | Scheduled | 12.02.2026 |

APPENDIX H

## Risk Management & FMEA Analysis

To ensure operational reliability and project continuity, the team employs a quantitative Failure Mode and Effects Analysis (FMEA) approach. Each risk is assigned a Probability (P) and Impact (I) score on a scale of 1 (Low) to 5 (Critical). The product of these factors yields the Risk Priority Number (RPN = P × I), which reflects the pre-mitigation (inherent) risk levels and dictates our mitigation focus. The mitigation strategies detailed in the subsequent columns are designed to reduce this residual risk to an acceptable ALARP (As Low As Reasonably Practicable) level.

The table below details the critical risks identified during the development cycle, specifically highlighting how our "Test Mule" strategy and simulation-free testing environment have been utilized as primary mitigation tools.

**Table H.1:** Risk Management Matrix (FMEA)

| Risk ID | Category | Risk Description | Prob. (P) | Impact (I) | RPN (PxI) | Mitigation Strategy (Prevention) | Contingency Plan (Recovery) |
|---|---|---|---|---|---|---|---|
| R-01 | Project | **Hull Manufacturing Delays:** The new 2026 composite hull design takes longer to manufacture than anticipated, delaying sea trials. | 5 | 5 | 25 | **"Test Mule" Strategy:** The complete 2026 electronics stack is validated on the Teknofest 2025 hull, decoupling software progress from mechanical dependencies. | Complete the competition using the retrofitted 2025 hull (Mule) if the new hull is not seaworthy by T-minus 2 weeks. |
| R-02 | Perception | **Visual False Negatives:** Failure to detect buoys due to extreme sun glare or water reflections. | 4 | 5 | 20 | **Real-World Training:** Dataset augmented with real reflection data collected in the Naval Academy harbor (no Sim-to-Real gap). Use of CPL (Circular Polarizing) filters. | The navigation stack prioritizes LIDAR point clouds over visual data when confidence scores drop below threshold. |
| R-03 | Electrical | **EMI & Signal Interference**: Data corruption caused by high-current motor harmonics and external RF congestion at the venue. | 4 | 4 | 16 | **Discrete Power Topology:** Physical separation of motor power lines from electronics; use of shielded cables and ferrite beads. | Aggressive digital filtering (Low-pass/Kalman) applied to sensor inputs to reject high-frequency noise spikes. |
| R-04 | Mechanical | **Water Ingress:** Seal failure due to gasket wear or assembly errors, leading to catastrophic short circuits in the electronics bay. | 3 | 5 | 15 | **IP68 & Vacuum Testing:** Use of marine-grade O-rings and polyurethane sealants on all joints. Pre-mission "Vacuum Leak Test" performed to verify hull integrity. | Telemetry monitoring via GCS real-time PDB voltage/current levels. Sudden power spikes indicate potential shorts/water drag, triggering an immediate manual recovery. |
| R-05 | Software | **Inference Latency (Lag):** Object detection algorithms (YOLO) consume excessive GPU resources, causing control loop delays. | 3 | 4 | 12 | **TensorRT Optimization:** Utilizing quantization (FP16) and caching techniques to reduce inference time on Jetson AGX Orin. | Switch to "Lightweight Mode" if under 7 FPS; Disable auxiliary logging and reduce camera resolution to 720p (< 7 FPS) or 480p (< 4 FPS) to free up GPU resources. |
| R-06 | Perception | **LIDAR False Positives:** Water spray from the shooter mechanism being detected as solid obstacles, causing the ASV to freeze or dodge phantom objects. | 3 | 4 | 12 | **Radius Outlier Removal:** Point cloud filters remove sparse points (spray) that do not have enough neighbors to be a solid object. | The software defines "Ignore Zones" in the LIDAR's field of view directly around the shooter nozzle outputs. |
| R-07 | Hardware | **Internal Data Link Failure:** Physical damage to Ethernet/USB interconnects or switch failure due to continuous hull vibration (fatigue) or impacts on obstacles. | 1 | 4 | 10 | **Strain Relief & Locking Connectors:** Implementation of strain relief loops on all cable harnesses; use of industrial latching connectors to prevent vibration-induced disconnection. | All internal cabling is modular (plug-and-play), not soldered directly. A "Rapid Field Repair Kit" with pre-crimped spares allows for <5 m replacement. \| |
| R-08 | Logistics | **Transit Damage (Florida):** Physical damage to the hull or sensitive sensors during international air freight to the competition venue. | 2 | 5 | 10 | **ATA-300 Flight Cases:** Packing critical systems in hard-shell cases with custom-cut foam inserts. LiPo batteries are transported in fireproof bags via carry-on per IATA regulations. | Essential sensors (Lidar/GPS) and Jetson modules are carried in cabin luggage to avoid rough handling in cargo. Epoxy repair kits are packed for hull fixes. |
| R-09 | Hardware | **Camera Impact Damage:** Physical destruction of the camera caused by accidental collision with floating obstacles or dock infrastructure. | 2 | 5 | 10 | **Protected Mounting Geometry:** The camera is mounted centrally and elevated, placing it effectively within a "geometric safety zone". | Rapid Swap Protocol: Quick-release mounts and a pre-calibrated spare camera unit allows for replacement in < 3 minutes between runs. |

| | | | | | | | |
|---|---|---|---|---|---|---|---|
| R-10 | Acoustics | **Signal-to-Noise Ratio (SNR) Drop:** Target pinger signals masked by wind-induced wave noise and ego-noise (thruster vibrations). | 3 | 3 | 9 | **Active DSP Filtering:** Implementation of High-Pass Filters (>20kHz) to reject low-frequency motor harmonics; FFT-based spectral subtraction. | “Stop-and-Listen" Protocol: The vehicle momentarily halts all thrusters to eliminate ego-noise, acquires the target frequency in silence, and resumes motion. |
| R-11 | Environmental | **Corrosion & Oxidation:** Saltwater vapor causing galvanic corrosion on exposed PCB traces and connector terminals over time. | 2 | 4 | 8 | **Conformal Coating:** Application of silicone-based protective coating on all PCBs; use of dielectric grease on all external connectors. | Rapid replacement of affected modules using pre-calibrated spares stored in desiccated (moisture-free) containers. |
| R-12 | GCS | **GCS Telemetry Lag:** Visualization latency (>500ms) on the ground control laptop due to high Wi-Fi packet traffic, causing "stuttering" on the operator's map. | 3 | 2 | 6 | **UI Thread Decoupling:** The Ground Control Station (GCS) software runs the rendering engine and data parsing on separate CPU threads to prevent UI freezing. | Since the ASV is fully autonomous, the operator relies on visual line-of-sight for status confirmation until the GUI catches up. |
| R-13 | Project | **Supply Chain Volatility:** Critical off-the-shelf components (sensors, thrusters, batteries) facing unexpected shipping delays or stock shortages. | 1 | 5 | 5 | **Diversified Sourcing (AVL):** Maintaining a pre-approved vendor list with primary and secondary suppliers for all critical BOM items; ordering "Long Lead Time" items immediately upon design freeze. | Mechanical interfaces and software drivers are designed to be generic, allowing rapid integration of alternative brands/models in case of stockouts. |
| R-14 | Safety | **Emergency Stop Failure:** Wireless kill switch fails to stop the boat due to signal interference. | 1 | 5 | 5 | **Redundant dual-band communication:** 2.4GHz + 900MHz Telemetry GCS, Failsafe logic stops motors upon signal loss >10000ms. | Physical E-Stop button located on the hull exterior for manual intervention by divers/safety boat. |
| R-15 | Management | **Workforce Attrition:** Loss of critical team members due to academic conflicts or unexpected leaves. | 1 | 4 | 4 | **Cross-Functional Training:** Adoption of a "T-shaped" skill model where members are trained in secondary disciplines to ensure redundancy. | All code and hardware schematics are documented in a central Confluence/Wiki page, allowing new members to onboard rapidly. |
| R-16 | GCS | **GCS Display Washout:** High ambient sunlight intensity causing poor visibility or glare on the Ground Control Station laptop screen during runs. | 3 | 1 | 3 | **Anti-Glare Hood:** Use of a foldable laptop sunshade (tent) and maximizing screen brightness settings for outdoor readability. | The operator shifts focus to Visual Line-of-Sight (VLOS), relying on the designated "Safety Spotter" to verbally confirm ASV movements and obstacle clearance. |
| R-17 | Data | **Non-Critical Log Truncation:** Onboard SSD/SD storage reaching capacity, preventing the saving of camera footage and debug data for post-mission analysis. | 2 | 1 | 2 | **Log Rotation Policy:** Implementation of a "Log Rotation" script that automatically deletes the oldest mission files to maintain free space**.** | The team utilizes the lower-resolution telemetry logs saved locally on the Ground Station laptop for debriefing analysis. |
| R-18 | Mechanical | **Cosmetic Decal Detachment:** Sponsor logos or team stickers peeling off due to water drag or prolonged sun exposure. | 1 | 1 | 1 | **Marine-Grade Vinyl:** Use of industrial adhesive vinyls with edge-sealing primer to prevent water lift. | No action required. The issue is purely aesthetic and has zero impact on hydrodynamic performance or mission success. |

As shown in Table H.1, high-RPN risks such as hull manufacturing delays (R-01) and perception failures (R-02) are mitigated through structural redundancies like the 'Test Mule' strategy and real-world data augmentation. The Risk Matrix below visualizes the distribution of these identified threats."

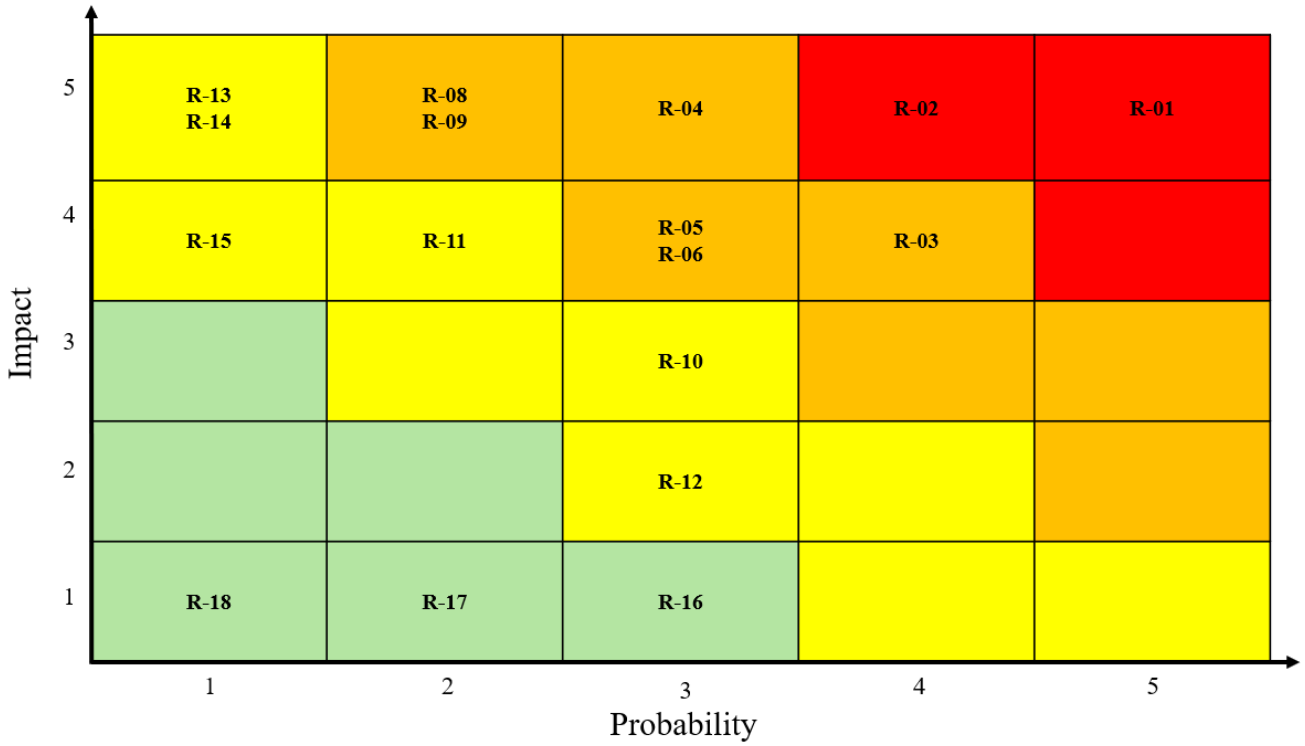


**Fig. H.1:** Risk Probability vs. Impact Matrix. The heatmap highlights the distinction between critical "Showstopper" risks (Red Zone) requiring architectural mitigation and manageable risks (Green Zone).